Analysis for integrated energy system

Zhang, Suhan; Gu, Wei; Zhang, Xiao-Ping; Chung, C. Y.; Yu, Ruizhi; Lu, Shuai; Palma-Behnke, Rodrigo

DOI:
10.1049/ein2.12002

Received: 20 January 2024 | Revised: 29 January 2024 | Accepted: 2 March 2024

Energy Internet

DOI: 10.1049/ein2.12002

WILEY

ORIGINAL RESEARCH

Analysis for integrated energy system: Benchmarking methods and implementation

Suhan Zhang[1] | **Wei Gu**[1] | **X.-P. Zhang**[2] | **C. Y. Chung**[3] | **Ruizhi Yu**[1] | **Shuai Lu**[1] | **Rodrigo Palma-Behnke**[4]

[1]School of Electrical Engineering, Southeast University, Nanjing, Jiangsu, China

[2]Department of Electronic, Electrical and Systems, University of Birmingham, Birmingham, UK

[3]Department of Electrical and Electronic Engineering, Hong Kong Polytechnic University, Hung Hom, Kowloon, Hong Kong

[4]Department of Electrical Engineering, Energy Center, University of Chile, Santiago, Chile

Correspondence

Wei Gu, School of Electrical Engineering, Southeast University, Nanjing, Jiangsu 210096, China.
Email: wgu@seu.edu.cn

Funding information

The National Science Fund for Distinguished Young Scholars, Grant/Award Number: 52325703; IEEE Power and Energy Society Working Group on Test Systems for Economic Analysis

Abstract

The selection of suitable models and solutions is a fundamental requirement for conducting energy flow analysis in integrated energy systems (IES). However, this task is challenging due to the vast number of existing models and solutions, making it difficult to comprehensively compare scholars' studies with current work. In this paper, we aim to address this issue by presenting a comprehensive overview of mainstream IES models and clarifying their relationships, thereby providing guidance for scholars in selecting appropriate models. Additionally, we introduce several widely used solvers for solving algebraic and differential equations, along with their detailed implementations in the energy flow analysis of IES. Furthermore, we conduct extensive testing and demonstration of these models and methods in various cases to establish benchmarking datasets. To facilitate reproducibility, verification and comparisons, we provide open-source access to these datasets, including system data, analysis settings and implementations of the various solvers in the mainstream models. Scholars can utilise the provided datasets to reproduce the results, verify the findings and perform comparative analyses. Moreover, they have the flexibility to customise these settings according to their specific requirements.

KEYWORDS

benchmarking method, energy flow analysis, integrated energy system, mainstream model, open-source data

1 | INTRODUCTION

1.1 | Background and motivations

Driven by escalating energy and environmental concerns, traditional energy systems are undergoing a transformation, characterised by increased renewable energy integration, enhanced energy efficiency and reduced carbon emissions.[1] However, most energy systems are currently designed, constructed and operated independently, which poses significant barriers to achieving coordination and exploiting synergies among them. For instance, the intermittency of renewable generation often leads to renewable energy curtailment. Nevertheless, by utilising energy conversion units, surplus electricity can be efficiently converted into gas or thermal power, which can then be utilised for gas supply or heating purposes. Moreover, the high demand for air conditioning during winter places substantial strain on the secure operation of the power system (PS). Nonetheless, by effectively managing the thermal inertia of buildings and heating networks, it is possible to reduce the electric load during peak periods without compromising user comfort. Integrated energy systems (IES) have emerged as a promising solution to address these challenges, as they facilitate the coordination of multiple energy flows to enhance energy efficiency and improve operational flexibility, garnering global attention.[2] To realise the aforementioned advantages, accurate and efficient methods for energy flow analysis including electricity, gas and heat are of paramount importance.

Formulating appropriate IES models and solving them under given conditions constitute two fundamental yet formidable tasks in energy flow analysis. However, these tasks

present significant challenges. From a physical perspective, the heterogeneous transport properties of multi-energy flows introduce multi-timescale dynamics within IES. Although independent energy subsystems are integrated at specific coupling units, the bidirectional energy flows give rise to mutual influences across various timescales, resulting in exceptionally complex combined analysis. From a mathematical standpoint, the IES model is described by high-dimensional partial differential–algebraic equations (PDAEs). Striking a balance between modelling accuracy and solution efficiency while ensuring convergence and stability poses a formidable challenge.[3]

1.2 | Literature review

In practical applications, the timescales of gas and heating systems (GS and HS) typically span from tens of minutes to hours. On the other hand, dynamic processes in the PS, such as electromagnetic and electromechanical transients, occur within microseconds to seconds, while static processes generally unfold over minutes. As a result, the PS primarily interacts with the GS and HS on a timescale of minutes. Therefore, the combined analysis predominantly focuses on the minute-level timescale and employs the static power flow model. In contrast, the GS and HS models are classified based on their respective timescales, giving rise to two types of energy flow analysis in IES, that is, static analysis and dynamic analysis.

Static energy flow analysis focuses on determining the state distribution at a single time step. By solving sets of algebraic equations (AEs) of static GS and HS models, static energy flow analysis is commonly used for medium- to long-term analysis like planning or assessment problems and providing initial values for dynamic analysis. In this regard, different solvers for AEs were employed for analysis. Reference 4 utilised the Newton–Raphson (NR) method to calculate energy flows in heat-electricity IES. Both decoupling and united solutions were developed to address the problem in IES with different coupling modes. Reference 5 extended the NR method to incorporate electricity-heat-gas IES. United solutions were adopted to solve the nonlinear problem and assess the impact of bidirectional energy flows. In reference 6, a fixed-point iteration method was proposed to solve static energy flow in a distributed manner. Similarly,[7] implemented a distributed calculation framework, employing the NR method and holomorphic embedding methods for calculations in different subsystems. To enhance the efficiency of the decomposed solution,[8,9] introduced the topological and component decoupling methods, respectively, to accelerate the iterative processes between different subsystems. These methods improved the efficiency of the decomposed solution.

Dynamic energy flow analysis focuses on capturing the effects of energy flow dynamics and their interdependencies across multiple time steps. By solving PDAEs of dynamic GS and HS models, dynamic energy flow analysis is commonly used for real-time problems like state estimation, simulation and economic dispatch. In the literature, references 10 and 11 employed the finite difference method (FDM) for energy flow optimisation. Specifically, central implicit schemes were used to discretise dynamic equations in GS and HS, respectively. In references 12 and 13, the Euler implicit schemes were utilised for discretisation, incorporating energy flow dynamics to facilitate renewable energy integration. Reference 14 proposed a unified formulation for the FDM-based analysis, where the transfer matrixes of initial and boundary conditions were derived to avoid the recursion and improve the efficiency. In reference 15, the method of characteristics (MOC) was employed to solve PDAEs and a sequential united method was developed to enhance the robustness and efficiency of the proposed PDAE solver. In addition to discretisation-based methods, another type of solver is based on function transformation. These methods transform the original partial differential equations (PDEs) into ordinary differential equations (ODEs) in function space. By making certain approximations, the ODEs in function space are solved and then inverse-transformed in the time domain. Representative function transformation methods for dynamic energy flow analysis include the Fourier transformation, Laplace transformation, differential transformation, etc. For instance, in references 16 and 17, the Fourier transformation was applied for dynamic analysis in GS and HS, representing the multi-energy states as combinations of different sinusoidal components. Reference 18 provides a comprehensive overview of the Fourier-based energy circuit method in energy management, discussing its implementation and applications. In references 19 and 20, the Laplace transformation was adopted to formulate the optimal energy flow problems in GS and HS. By algebraizing the PDEs using the Laplacian operator, the energy flow problems were effectively addressed. The circuit-analogue method based on the Laplace transformation, along with its applications in low carbon analysis, is summarised in reference 21. In references 22 and 23, the differential transformation was employed to reformulate the AEs in PS and the PDAEs in HS, respectively. This approach enabled the expression of nonlinear equation sets in IES as recursive equation sets, thereby avoiding the need for iterations. Contrasting with the aforementioned studies focusing on energy flow, reference 24 analysed the exergy distribution in IES and proposed a generalised framework for exergy flow calculation.

Comparative methods for IES analysis are essential for method verification and performance evaluation. However, researchers often face challenges in selecting appropriate benchmarking methods and conducting comprehensive analyses due to several reasons. Firstly, some simulation settings are tailored to specific requirements and may not be easily transferred to other scenarios with similar performance. For example, the MOC accurately solves PDEs but requires small time step sizes, making it unsuitable for systems with short pipelines due to stability constraints.[3] Secondly, many research papers only present selected simulation results for illustration and comparison, while detailed results are unavailable in the manuscripts. This can lead to a biased comparison between the proposed approach and existing methods. Thirdly, the lack of open-source benchmarking data and simulation settings in

many research papers makes it challenging to reproduce and validate the proposed work. Although some studies provide benchmarking data for IES analysis,[25] they are primarily designed for static analysis and the necessary dataset for dynamic analysis, such as initial conditions and initial guesses, is often lacking. To address these challenges, it is crucial for researchers to establish standardised benchmarking datasets and simulation settings that cover a wide range of IES scenarios. Open-sourcing such data would facilitate fair and comprehensive comparisons between different methods and promote reproducibility in the field of IES analysis.

1.3 | Contributions and paper organization

To fulfil the mentioned gaps, three targets are raised in this paper. The first target is introducing different IES models and comprehensively characterising their correlations. The second target is to reproduce mainstream solvers for energy flow analysis in different IESs, thereby providing benchmarking methods and simulation results for future verification. Finally, with the benchmarking methods, we comprehensively compare various IES models to clarify their applicable scope. We aim to provide scholars with the open-source dataset and method sheet rather than give preferences to specific models or solvers. The main contributions of this paper are summarised as follows.

1. We provide detailed datasets for static and dynamic analysis of IES, including the system data, simulation settings and method parameters.
2. We provide the implementation of the benchmarking methods. A sheet of mainstream methods is comprehensively investigated.
3. We provide a performance comparison of the benchmarking methods with their detailed simulation results. The comparison is implemented in several IESs with different simulation settings.

The remainder of this paper is as follows. Different IES models are introduced in Section 2. The benchmarking methods for static and dynamic analysis are given in Sections 3 and 4, respectively. Sections 5 and 6 present the case studies for model comparisons and methods implementation, respectively. Section 7 is finalised with a conclusion.

2 | FORMULATION OF IES MODELS

2.1 | Models of PS

At the timescale of minutes during regular operation, the AC power flow is commonly adopted to describe electric power flow distribution at buses and branches, as shown below.

$$P_{Gi} - P_{Li} = U_i \sum_j U_j \left(G_{ij} \cos\theta_{ij} + B_{ij} \sin\theta_{ij}\right) \quad i,j \in \Theta_e \quad (1)$$

$$Q_{Gi} - Q_{Li} = U_i \sum_j U_j \left(G_{ij} \sin\theta_{ij} - B_{ij} \cos\theta_{ij}\right) \quad i,j \in \Theta_e \quad (2)$$

$$P_{l,ij} = U_i U_j \left(G_{ij} \cos\theta_{ij} + B_{ij} \sin\theta_{ij}\right) - G_{ij} U_i^2 \quad i,j \in \Theta_e \quad (3)$$

$$Q_{l,ij} = U_i U_j \left(G_{ij} \sin\theta_{ij} - B_{ij} \cos\theta_{ij}\right) + B_{ij} U_i^2 \quad i,j \in \Theta_e \quad (4)$$

where P_G and P_L are the active power generation and consumption; U and θ are the voltage magnitude and phase angle; P_l and Q_l are the active and reactive branch power flow; B and X are the susceptance and reactance; Θ_e is the bus set in the PS.

2.2 | Models of GS

2.2.1 | *GS-Model1*

Assuming that the gas flow transportation is the isothermal process and the pipeline inclination is zero, the continuity and momentum equations and state equations are used to model the gas flow dynamics, as shown below.

$$\frac{\partial \rho}{\partial t} + \frac{\partial (\rho v)}{\partial x} = 0 \quad (5)$$

$$\frac{\partial (\rho v^2)}{\partial x} + \frac{\partial (\rho v)}{\partial t} + \frac{\partial p}{\partial x} + \frac{\lambda_g \rho v^2}{2D} = 0 \quad (6)$$

$$p = \rho c^2 \quad (7)$$

where p is the pressure, Pa; ρ is the density, kg/m^3; v is the flow velocity, m/s; D is the pipeline diameter, m; g is the gravity acceleration, m/s^2; λ_g is the friction factor of the gas pipeline. The continuity Equation (5) represents mass conservation, where the first and second terms denote mass change and flux increment. The momentum Equation (6) represents momentum conservation, where the four terms represent the momentum increment caused by convection, acceleration, surface stress and friction resistance. Equation (7) is the ideal state equation in an isothermal process. Moreover, the density and flow velocity are linked in the following equation.

$$q = Sv\rho \quad (8)$$

where S is the cross-section area of the pipeline, m^2; q is the mass flow rate, kg/s. Replacing ρ with q, Equations (5) and (6) can be rewritten as:

$$\frac{\partial p}{\partial t} + \frac{c^2}{S}\frac{\partial q}{\partial x} = 0, \frac{c^2}{S^2}\frac{\partial}{\partial t}\left(\frac{q^2}{p}\right) + \frac{\partial p}{\partial x} + \frac{1}{S}\frac{\partial q}{\partial t} + \frac{\lambda_g c^2 q^2}{2DS^2 p} = 0 \quad (9)$$

Besides the distribution along the pipeline, the gas states should also satisfy the conservation law at the junctions, as shown below.

$$p_b^{\mathrm{o}} - p_{nd,k} = 0, p_n^{\mathrm{i}} - K_{cp,k} p_{nd,k} = 0 \quad b \in \Phi_{g,k}^{\mathrm{o}}, n \in \Phi_{g,k}^{\mathrm{i}} \quad (10)$$

$$\sum_b q_b^{\mathrm{o}} - \sum_j q_j^{\mathrm{i}} - q_{nd,k} = 0 \quad k \in \Theta_g, b \in \Phi_{g,k}^{\mathrm{o}}, j \in \Phi_{g,k}^{\mathrm{i}} \quad (11)$$

where q_{nd} is the node mass flow rate, kg/s; p_{nd} is the node pressure, Pa; $K_{cp,k}$ is the compression ratio if node k is a compressor, else, $K_{cp,k} = 1$; superscripts 'i' and 'o' are the symbols of inlet and outlet variables; $\Phi_{g,k}^{\mathrm{o}}$ and $\Phi_{g,k}^{\mathrm{i}}$ are the sets of pipelines ending and starting at node k in the GS; Θ_g is the node set in the GS.

Since the *GS-Model1* is too complex for analysis, certain simplifications should be fitted to the given conditions, deriving the following four mainstream models.

2.2.2 | *GS-Model2*

Neglecting the convection terms in Equation (9), we have:

$$\frac{\partial p}{\partial t} + \frac{c^2}{S}\frac{\partial q}{\partial x} = 0, \frac{\partial p}{\partial x} + \frac{1}{S}\frac{\partial q}{\partial t} + \frac{\lambda_g c^2 q^2}{2DS^2 p} = 0 \quad (12)$$

Meanwhile, Equations (10) and (11) in *GS-Model1* remains unchanged in *GS-Model2*.

2.2.3 | *GS-Model3*

Further neglecting the acceleration terms of the momentum equation in (12), *GS-Model3* is expressed as:

$$\frac{\partial p}{\partial t} + \frac{c^2}{S}\frac{\partial q}{\partial x} = 0, \frac{\partial p}{\partial x} + \frac{\lambda_g c^2 q^2}{2DS^2 p} = 0 \quad (13)$$

Besides, Equations (10) and (11) in *GS-Model1* remain unchanged.

2.2.4 | *GS-Model4 & 5*

The nonlinearity in Equation (12) makes the analysis challenging. To address this issue, some studies employ methods such as the average flow velocity to linearise the model, thereby avoiding convergence and complexity issues while maintaining certain accuracy. Correspondingly, *GS-Model2 and GS-Model3* are linearised as follows.

$$\frac{\partial p}{\partial t} + \frac{c^2}{S}\frac{\partial q}{\partial x} = 0, \frac{\partial p}{\partial x} + \frac{1}{S}\frac{\partial q}{\partial t} + \frac{\lambda_g w q}{2DS} = 0 \quad (14)$$

$$\frac{\partial p}{\partial t} + \frac{c^2}{S}\frac{\partial q}{\partial x} = 0, \frac{\partial p}{\partial x} + \frac{\lambda_g w q}{2DS} = 0 \quad (15)$$

where w is the pre-defined average flow velocity, m/s. Also, Equations (10) and (11) in *GS-Model1* remain unchanged in *GS-Model4 and GS-Model5*.

2.2.5 | *GS-Model6*

At a larger timescale, the gas flow dynamics turn to be static. In this condition, Equation (12) can be rewritten into AEs by neglecting the differential terms regarding t.

$$\begin{cases} \dfrac{\mathrm{d}q}{\mathrm{d}x} = 0 \Rightarrow q = \text{constant} \\ \dfrac{\mathrm{d}p}{\mathrm{d}x} + \dfrac{\lambda_g c^2 q^2}{2DS^2 p} = 0 \end{cases} \Rightarrow \begin{cases} (p^{\mathrm{o}})^2 - (p^{\mathrm{i}})^2 - K_g q^2 = 0 \\ K_g = \dfrac{\lambda_g c^2 L}{DS^2} \end{cases} \quad (16)$$

Substituting (10) into (16), all the pipeline pressures in *GS-Model6* can be replaced with node pressures. Therefore, Equation (16) can be rewritten as follows, while Equation (11) remains unchanged.

$$p_{nd,k}^2 - p_{nd,n}^2 = K_{g,i} q_i^2 \quad i \in \Phi_g, k \in \Theta_{g,i}^+, n \in \Theta_{g,i}^- \quad (17)$$

where $\Theta_{g,i}^+$ and $\Theta_{g,i}^-$ are the nodes at the inlet and outlet of pipeline i in the GS. The features of different GS models are summarised in Table 1.

2.3 | Models of HS

The HS is a two-layer system composed of supply and return networks, wherein the thermal power is carried by the hot water flow. According to the regulation mode, the HS models can be categorised into two types. The first type of HS model corresponds to the quantity regulation mode. Under quantity regulation mode, the operators adjust the mass flow rate to satisfy the thermal load, causing the hydraulic and thermal coupling in the HS model. Another type corresponds to the quality regulation model. Under this mode, the operators adjust the water temperature while fixing the mass flow rate. Consequently, the HS model under quality regulation only contains thermal parts.

2.3.1 | Hydraulic model

According to reference 26, the pressure and flow changes over 1000 times faster than the temperature variation. The hydraulic dynamics are considered to be of less significance compared with the thermal dynamics. Therefore, the hydraulic model is built in a static form, containing flow continuity equation in (18), loop pressure equation in (19) and pressure loss equation in (20).

TABLE 1 Summary of current integrated energy system models.

Model	Formulas	Static/dynamic	Nonlinear/linear
PS-Model	(1)–(4)	Static	Nonlinear
GS-Model1	(9)–(11)	Dynamic	Nonlinear
GS-Model2	(10)–(12)	Dynamic	Nonlinear
GS-Model3	(10), (11), (13)	Dynamic	Nonlinear
GS-Model4	(10), (11), (14)	Dynamic	Linear
GS-Model5	(10), (11), (15)	Dynamic	Linear
GS-Model6	(11), (17)	Static	Nonlinear
HS-Model1	(18)–(24)	Dynamic	Nonlinear
HS-Model2	(18)–(20), (22)–(24), (25)	Static	Linear in quality regulation; nonlinear in quantity regulation
HS-Model3	(18)–(20), (22)–(24), (26)	Dynamic	
HS-Model4	(18)–(20), (22)–(24), (27)	Dynamic	

$$\boldsymbol{A}\boldsymbol{m} = \boldsymbol{m}_{nd} \tag{18}$$

$$\boldsymbol{B}\Delta\boldsymbol{p} = \boldsymbol{0} \tag{19}$$

$$\Delta p_i = K_{f,i} m_i |m_i| \quad i \in \Phi_h \tag{20}$$

where $\boldsymbol{A}$ is the node-branch incidence matrix, $a_{ij} = 1/-1$ if node i locates the inlet/outlet of pipeline j, else, $a_{ij} = 0$; $\boldsymbol{m}$ is the vector of pipeline mass flow rate in the HS, kg/s; $\boldsymbol{m}_{nd}$ is the vector of node mass flow rate in the HS, kg/s; $\boldsymbol{B}$ is the loop-branch incidence matrix, $b_{ij} = 1/-1$ if the loop i has the same/reverse direction as pipeline j, else, $b_{ij} = 0$; K_f is the lumped pipeline resistance coefficient; $\Delta\boldsymbol{p}$ is the vector of pipeline pressure drop; Φ_h is the set of pipelines in the HS.

2.3.2 | *HS-Model1*

Besides the hydraulic model, the thermal model is another part of the HS model. Firstly, the pipeline temperature should satisfy the energy conservation law. Neglecting the fluid heat conduction, the corresponding equation is expressed as:

$$\frac{\partial T}{\partial t} + v\frac{\partial T}{\partial x} + \frac{v}{C_w m \lambda_h} T = 0 \tag{21}$$

where T is the pipe temperature that takes ambient temperature as the reference, °C; C_w is the water specific heat capacity, J/(kg · °C); λ_h is the pipeline thermal resistance. The terms on the left side of Equation (21) represent the temperature variation of an infinitesimal element caused by the inner energy change, transverse heat input and radial heat loss, respectively.

Secondly, the hot water flow mixing at the nodes should also satisfy the energy conservation law, thereby deriving the following temperature mixing equation.

$$T_{nd,k}\sum_b m_b = \sum_j m_j T_j^{\mathrm{o}} \quad k \in \Theta_h, b \in \Phi_{h,k}^{\mathrm{i}}, j \in \Phi_{h,k}^{\mathrm{o}} \tag{22}$$

where Θ_h is the set of nodes in the HS; $\Phi_{h,k}^{\mathrm{o}}$ and $\Phi_{h,k}^{\mathrm{i}}$ are the sets of pipelines ending and starting at node k in the HS; T_{nd} is the node temperature.

Thirdly, the node and pipeline inlet temperatures should satisfy the continuity equation, as shown below.

$$T_j^{\mathrm{i}} = T_{nd,k} \quad k \in \Theta_h, j \in \Phi_{h,k}^{\mathrm{i}} \tag{23}$$

Fourthly, the supply and return temperatures are linked in Equation (24), which describes the thermal power at nodes.

$$\phi_i = C_w m_{nd,i}\left(T_{nd,i}^{s} - T_{nd,i}^{r}\right) \quad k \in \Theta_h \tag{24}$$

where T_{nd}^{s} and T_{nd}^{r} are the node supply and return temperatures, respectively; ϕ is the thermal power.

2.3.3 | *HS-Model2*

Neglecting the temperature variation regarding t, Equation (21) can be simplified as:

$$\frac{\mathrm{d}T}{\mathrm{d}x} + \frac{T}{C_w m \lambda_h} = 0 \Rightarrow T^{\mathrm{o}} = T^{\mathrm{i}} e^{\frac{-L}{C_w m \lambda_h}} \tag{25}$$

where L is the pipeline length, m. Similarly, the other equations in *HS-Model2* are the same as those in *HS-Model1*.

2.3.4 | *HS-Model3*

Different from the above models deriving from the PDE, *HS-Model3* directly models the time delay and thermal loss in the HS and is called lumped model,[26] as shown below.

$$T_t^{\mathrm{o}} = T_{t-\xi_{lp}}^{\mathrm{i}} e^{\frac{-L}{C_w m \lambda_h}} \quad \xi_{lp} = \left\lfloor \frac{L}{v\Delta t} \right\rfloor \tag{26}$$

where Δt is the time step size, ξ_{lp} is the pipeline time delay in *HS-Model3*. Meanwhile, hydraulic equations, temperature mixing equation, temperature continuity equation and thermal power equation of *HS-Model2* are the same as those in *HS-Model1*.

2.3.5 | *HS-Model4*

Another technique to model HS is the node method, which is defined as *HS-Model4*. In *HS-Model4*, the mass flow along the pipeline is discretised into multiple blocks. Then, the outlet temperature is computed by averaging the historical inlet temperature with certain loss coefficients. The typical formula of *HS-Model4* is expressed as:

$$T_t^{\mathrm{o}} = K_{NM} \sum_{k=t-\xi_{1t}}^{t-\xi_{2t}} T_{t-k}^{\mathrm{i}} \tag{27}$$

where K_{NM} is the transfer coefficient; ξ_{1t} and ξ_{2t} are the labels of time delay in *HS-Model4*. The formulas of K_{NM}, χ_{1t} and χ_{2t} are given in reference 26.

Except for Equations (27), (18)–(20) and (23), (24) in *HS-Model4* are the same as those in *HS-Model1*. The features of different HS models are summarised in Table 1.

2.4 | Models of coupling units

The coupling units in IESs contain the energy conversion and cogeneration device. Typical cogeneration devices include the back-pressure and extraction combined heat and power (CHP) units, whose models are listed below.

$$\phi_{bp} = \eta_{bp} P_{bp} \tag{28}$$

$$\eta_{ec} = \frac{\phi_{ec} - \phi_{ec,base}}{P_{ec,base} - P_{ec}} \tag{29}$$

where subscripts '*bp*' and '*ec*' are the symbols of back pressure and extraction CHP units; η is the thermal-electric coefficient; ϕ_{base} and P_{base} are the rated thermal and electric power output of the extraction CHP units.

Typical energy conversion devices include the electric boilers (EB), heat pumps (HP), gas turbines (GT) and power to gas (P2G) facilities. The EB and HP consume the electric power to generate thermal power, whose models are:

$$\phi_{eb} = \eta_{eb} P_{eb}, \phi_{hp} = \eta_{hp} P_{hp} \tag{30}$$

where subscripts '*eb*' and '*hp*' are the symbols of EB and HP; η_{eb} and η_{hp} are the efficiencies of EB and HP. The GT consumes gas flow to generate electric power, while the P2G transforms the abundant electric power to generate gas flow. Their models are:

$$P_{gt} = \eta_{gt} q_{gt} h_g, q_{pg} = \frac{\eta_{pg} P_{pg}}{h_g} \tag{31}$$

where subscripts '*gt*' and '*pg*' are the symbols of GT and P2G, respectively; η_{gt} and η_{pg} are the efficiencies of GT and P2G; h_g is the calorific value of gas.

3 | BENCHMARKING METHODS FOR ENERGY FLOW ANALYSIS

According to Table 1, dynamics and nonlinearity are two main features when utilising the IES model for analysis. A common method to handle these problems is to algebraise PDEs and then solve the obtained AEs jointly.

3.1 | Solutions for PDEs

This section selects the FDM with the Euler implicit scheme (M1), FDM with central implicit scheme (M2) and MOC as the benchmarking PDE solvers. The selection of these methods is based on the following criteria:

1. *Applicability*: The three methods are highly applicable and suitable for both linear and nonlinear cases, making them versatile choices for solving a wide range of PDE problems.
2. *Incorporation of initial and boundary conditions*: All three methods can explicitly incorporate the initial and boundary conditions of the PDEs under consideration. This ensures that the solvers can accurately capture the behaviour of the system at the initial time and along the boundaries.
3. *Uniform format*: The formats of simulation settings in the three methods are the same. This uniformity allows for establishing comparative trials in a more convincing manner, as it simplifies the process of evaluating and comparing the performance of the different solvers.

For simplification, the PDEs in Section 3 are summarised into the following united form.

$$\boldsymbol{K}_1 \frac{\partial \boldsymbol{u}}{\partial x} + \boldsymbol{K}_2 \frac{\partial \boldsymbol{u}}{\partial t} = \boldsymbol{K}_3 \boldsymbol{y}(\boldsymbol{u}) \tag{32}$$

where $\boldsymbol{u}$ is the vector of state variables to be solved in the PDEs; $\boldsymbol{K}_1$–$\boldsymbol{K}_3$ are the constant coefficient matrixes; $\boldsymbol{y}(\boldsymbol{u})$ is the function of $\boldsymbol{u}$.

3.1.1 | Finite difference method

The main steps of FDM are as follows.

1. *Grid division*. The solution domain is divided into a series of discrete points to form a grid. Uniform grids are usually used, as shown below.

$$\Delta t = \frac{\Gamma}{N_t}, \Delta x = \frac{L}{N_x} \tag{33}$$

where Δx is the space step size; N_x and N_t are the numbers of the space and time steps; Γ is the length of the time period.

2. *Difference approximation*. At discrete points, the derivatives are approximated with certain difference quotients. In M1, the backward difference quotient is used for approximation, as shown below.

$$\begin{cases} \dfrac{\partial \boldsymbol{u}_{i+1}^{j+1}}{\partial t} \simeq \dfrac{\boldsymbol{u}_{i+1}^{j+1} - \boldsymbol{u}_{i+1}^{j}}{\Delta t} & \\ \dfrac{\partial \boldsymbol{u}_{i+1}^{j+1}}{\partial x} \simeq \dfrac{\boldsymbol{u}_{i+1}^{j+1} - \boldsymbol{u}_{i}^{j+1}}{\Delta x} & \begin{matrix} 0 \le i \le N_x \\ 0 \le i \le N_t \end{matrix} \\ \boldsymbol{y}\left(\boldsymbol{u}_{i+1}^{j+1}\right) = \boldsymbol{y}\left(\boldsymbol{u}_{i+1}^{j+1}\right) & \end{cases} \tag{34}$$

In M2, the central difference quotient is used for approximation, as shown below.

$$\begin{cases} \dfrac{\partial \boldsymbol{u}_{i+0.5}^{i+0.5}}{\partial t} \simeq \dfrac{\boldsymbol{u}_{i}^{j+1} + \boldsymbol{u}_{i+1}^{j+1} - \boldsymbol{u}_{i}^{j} - \boldsymbol{u}_{i+1}^{j}}{2\Delta t} & 0 \le i \le N_x \\ \dfrac{\partial \boldsymbol{u}_{i+0.5}^{i+0.5}}{\partial x} \simeq \dfrac{\boldsymbol{u}_{i+1}^{j} + \boldsymbol{u}_{i+1}^{j+1} - \boldsymbol{u}_{i}^{j} - \boldsymbol{u}_{i}^{j+1}}{2\Delta x} & 0 \le j \le N_t \\ \boldsymbol{y}\left(\boldsymbol{u}_{i+0.5}^{i+0.5}\right) \simeq \dfrac{\boldsymbol{y}\left(\boldsymbol{u}_{i}^{j+1}\right) + \boldsymbol{y}\left(\boldsymbol{u}_{i+1}^{j+1}\right) + \boldsymbol{y}\left(\boldsymbol{u}_{i}^{j}\right) + \boldsymbol{y}\left(\boldsymbol{u}_{i+1}^{j}\right)}{4} & \end{cases} \tag{35}$$

3. *Form a difference equation set*. Replace the derivatives in the PDE with the approximations. Then, the PDE is discretised into a system of AEs.
4. *Solve the AE set*. Combining with the initial and boundary conditions, the numerical solution is obtained by solving the AE sets.

3.1.2 | Method of characteristics

The main steps of MOC are as follows.[27]

1. *Determine and solve the characteristic equation*. This is obtained by constructing total differentiation of $\boldsymbol{u}$.

$$\frac{d\boldsymbol{u}}{dt} = \frac{dx}{dt}\frac{\partial \boldsymbol{u}}{\partial x} + \frac{\partial \boldsymbol{u}}{\partial t}, \quad \frac{dx}{dt} = \frac{\boldsymbol{K}_1}{\boldsymbol{K}_2} \tag{36}$$

2. *Transform the PDE into ODE along the characteristic line*. Substituting the characteristic equation with the original PDE, the ODE along the characteristic line is then obtained.

$$\frac{d\boldsymbol{u}}{dt} = \frac{\boldsymbol{K}_3}{\boldsymbol{K}_2}\boldsymbol{y}(\boldsymbol{u}), \quad \frac{dx}{dt} = \frac{\boldsymbol{K}_1}{\boldsymbol{K}_2} \tag{37}$$

3. *Solve the ODEs along the characteristic line*. The ODEs are solved along each characteristic line to obtain the solution.
4. *Reconstruct the solution*. Finally, the solutions along the characteristic curves are combined to reconstruct the solution in the original domain.

3.2 | Solutions for AEs

After algebraizing the PDEs, only AEs remain unsolved in energy flow analysis, as shown in Equation (38).

$$\boldsymbol{f}(\boldsymbol{u}) = \boldsymbol{0} \tag{38}$$

where $\boldsymbol{f}$ is the AE set of IES models in Table 1.

A typical solver for nonlinear AE sets is the NR method. The corresponding iterative equation, unbalanced vector and convergence condition of the NR method are as follows.

$$\begin{cases} \Delta \boldsymbol{u}^{(k)} = \left(\boldsymbol{J}^{(k)}\right)^{-1} \Delta \boldsymbol{f}^{(k)} \\ \boldsymbol{u}^{(k+1)} = \Delta \boldsymbol{u}^{(k)} + \Delta \boldsymbol{u}^{(k)} \\ \left|\Delta \boldsymbol{u}^{(k)}\right| \le \varepsilon \end{cases} \tag{39}$$

where superscript (k) is the number of iterations; ε is the convergence limit; $\boldsymbol{J}$ is the Jacobian matrix of the AE set; $\Delta \boldsymbol{u}$ and $\Delta \boldsymbol{f}$ are the unbalanced vectors of the state variables and equations.

As for the linear AE set, the solution can be directly obtained using matrix inversion, as shown below.

$$\boldsymbol{u} = \boldsymbol{J}^{-1}\boldsymbol{f} \tag{40}$$

4 | METHOD IMPLEMENTATION IN STATIC ANALYSIS

4.1 | Analysis in PS

It is assumed that there are N_e buses in the PS, including N_{e1} PQ buses, N_{e2} PV buses and one slack bus. In this condition, $N_e - 1$ phase angle and N_{e1} voltage magnitude are to be solved. Correspondingly, $N_e - 1$ set of (1) can be built for active power balance at PV and PQ buses, N_{e1} set of (2) can be built for reactive power balance at PQ buses. Since the numbers of variables and equations are the same, the closure of the equation set in the PS is guaranteed. Substituting the PS model into (39), we have:

$$\boldsymbol{u}_e = [\,\boldsymbol{U} \quad \boldsymbol{\theta}\,]^{\mathrm{T}}, \boldsymbol{f}_e = [\,\boldsymbol{f}_{e1} \quad \boldsymbol{f}_{e2}\,]^{\mathrm{T}} \tag{41}$$

$$\boldsymbol{J}_e = \begin{bmatrix} \partial \boldsymbol{f}_{e1} / \partial \boldsymbol{U} & \partial \boldsymbol{f}_{e1} / \partial \boldsymbol{\theta} \\ \partial \boldsymbol{f}_{e2} / \partial \boldsymbol{U} & \partial \boldsymbol{f}_{e2} / \partial \boldsymbol{\theta} \end{bmatrix} \tag{42}$$

where $\boldsymbol{U}$ is the vector of voltage magnitude of PQ buses; $\boldsymbol{\theta}$ is the vector of phase angle of PV and PQ buses; $\boldsymbol{f}_{e1}$ is the active power balance equation at PV and PQ buses; $\boldsymbol{f}_{e2}$ is the reactive power balance equation at PQ bus. The detailed expressions of $\boldsymbol{J}_e$ can be found in reference 15.

4.2 | Analysis in GS

Static analysis in GS refers to the utilisation of *GS-Model6*. Similar to the PS analysis, the nodes in the GS are classified into two types according to the known and unknown variables. As shown in Table 2, the first type corresponds to the gas sources with known pressures, the second type corresponds to the gas loads with known mass flow rates.

Assuming that there are N_g nodes and N_{b1} pipelines in the GS, the variable distribution is presented in Figure 1 including N_g node pressures, N_g node mass flow rates and $2N_{b1}$ pipeline mass flow rates. Correspondingly, N_g set of (11) for mass conservation at nodes (defined as $\boldsymbol{f}_{g1}$) and N_{b1} set of (16) for pipeline equations (defined as $\boldsymbol{f}_{g2}$) can be built. To ensure the closure, N_{b1} boundary conditions are needed, as shown in Equation (43) (defined as $\boldsymbol{f}_{g3}$).

$$\begin{cases} p_{nd,i} - \varphi_{gp,i} = 0 \\ q_{nd,j} - \varphi_{gq,j} = 0 \end{cases} \quad i \in \Theta_g^{sr}, j \in \Theta_g^{ld} \tag{43}$$

where Θ_g^{sr} and Θ_g^{ld} are the sets of source and load nodes in the GS, φ_{gp} and φ_{gq} are the boundary conditions of node pressures and mass flow rates.

With these settings, the expressions of (39) in static gas flow analysis are as follows.

$$\boldsymbol{u}_g = [\boldsymbol{p}_{nd} \quad \boldsymbol{q} \quad \boldsymbol{q}_{nd}]^{\mathrm{T}}, \boldsymbol{f}_g = [\boldsymbol{f}_{g1} \quad \boldsymbol{f}_{g2} \quad \boldsymbol{f}_{g3}]^{\mathrm{T}} \tag{44}$$

$$\boldsymbol{J}_g = \begin{bmatrix} \mathbf{0} & \mathbf{A} & -\mathbf{1} \\ \partial \boldsymbol{f}_{g2} / \partial \boldsymbol{p}_{nd} & \partial \boldsymbol{f}_{g2} / \partial \boldsymbol{q} & \mathbf{0} \\ \partial \boldsymbol{f}_{g3} / \partial \boldsymbol{p}_{nd} & \mathbf{0} & \partial \boldsymbol{f}_{g3} / \partial \boldsymbol{q}_{nd} \end{bmatrix} \tag{45}$$

TABLE 2 Node variable distribution in gas system.

Node type	Known variables	Unknown variables
Source node	p_{nd}	q_{nd}
Load node	q_{nd}	p_{nd}

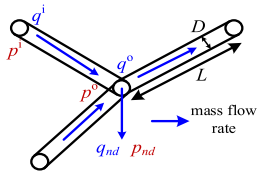

FIGURE 1 Variable distribution in the gas system.

4.3 | Analysis in HS

Static analysis in HS refers to the utilisation of *HS-Model3* and is further characterised by regulation mode. It is assumed that there are N_h nodes, N_{h2} pipelines and N_l loops in the HS, including N_{h1} source nodes, N_{h2} intermediate nodes and N_{h3} load nodes ($N_h = N_{h1} + N_{h2} + N_{h3}$).

4.3.1 | Quality regulation

The variables in quality-regulated HSs contain N_h node thermal power, $2N_h$ node supply and return temperatures, $2N_{h2}$ pipeline inlet and outlet temperatures in the supply network and $2N_{h2}$ pipeline inlet and outlet temperatures in the return network. The variable distribution in the HS is shown in Figure 2. Similarly, the nodes in quality-regulated HS are classified into three types for clarification, as shown in Table 3. Types I and II correspond to the source nodes for power and temperature regulation, respectively. Type III corresponds to the load and intermediate nodes.

Accordingly, $N_h + N_{h2}$ sets of (22) can be built for energy conservation at nodes (defined as $\boldsymbol{f}_{h1}$), including $N_{h1} + N_{h2}$ sets in the supply network and $N_{h2} + N_{h3}$ sets in the return network. $2N_{h2}$ set of (23) (defined as $\boldsymbol{f}_{h2}$) and $2N_{h2}$ sets of (26) (defined as $\boldsymbol{f}_{h3}$) can be built for pipeline temperature. $N_h - N_{h2}$ sets of (24) can be built for thermal power at source and load nodes (defined as $\boldsymbol{f}_{h4}$). Thus, N_h sets of boundary conditions (defined as $\boldsymbol{f}_{h5}$) are needed as follows, where Θ_h^{sl} is the set of Type I nodes in the HS, φ_{hT} and $\varphi_{h\phi}$ are the boundary conditions of node supply temperature and thermal power.

$$\begin{cases} T^{s}_{nd,i} - \varphi_{hT,i} = 0 & i \in \Theta_h^{sl} \\ \phi_{nd,j} - \varphi_{h\phi,j} = 0 & j \in \Theta_h, j \notin \Theta_h^{sl} \end{cases} \tag{46}$$

In the energy flow analysis of the HS, two methods are developed, including the united method and decoupling method. The former constructs a high-dimensional equation set and solves all the equations together. The latter solves the equations in supply and return networks separately and converges through iteration. In the united methods, the elements in Equation (40) are shown below.

$$\begin{cases} \boldsymbol{u}_h = [\boldsymbol{T}^{s}_{nd} \quad \boldsymbol{T}^{r}_{nd} \quad \boldsymbol{T}^{\mathrm{i},s} \quad \boldsymbol{T}^{\mathrm{o},s} \quad \boldsymbol{T}^{\mathrm{i},r} \quad \boldsymbol{T}^{\mathrm{o},r} \quad \boldsymbol{\phi}]^{\mathrm{T}} \\ \boldsymbol{f}_h = [\boldsymbol{f}_{h1} \quad \boldsymbol{f}_{h2} \quad \boldsymbol{f}_{h3} \quad \boldsymbol{f}_{h4} \quad \boldsymbol{f}_{h5}]^{\mathrm{T}} \end{cases} \tag{47}$$

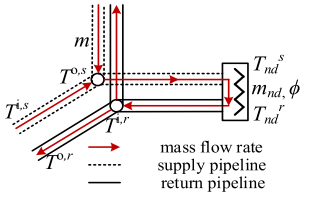

FIGURE 2 Variable distribution in the heating system.

TABLE 3 Node variable distribution in quality-regulated heating system.

Node type	Known variables	Unknown variables
Type I	T^s_{nd}	T^r_{nd}, ϕ
Type II	ϕ	T^s_{nd}, T^r_{nd}
Type III	ϕ	T^s_{nd}, T^r_{nd}

$$\boldsymbol{J}_h = \begin{bmatrix} \frac{\partial \boldsymbol{f}_{h1}}{\partial \boldsymbol{T}^s_{nd}} & \frac{\partial \boldsymbol{f}_{h1}}{\partial \boldsymbol{T}^r_{nd}} & \mathbf{0} & \frac{\partial \boldsymbol{f}_{h1}}{\partial \boldsymbol{T}^{o,s}} & \mathbf{0} & \frac{\partial \boldsymbol{f}_{h1}}{\partial \boldsymbol{T}^{o,r}} & \mathbf{0} \\ \frac{\partial \boldsymbol{f}_{h2}}{\partial \boldsymbol{T}^s_{nd}} & \frac{\partial \boldsymbol{f}_{h2}}{\partial \boldsymbol{T}^r_{nd}} & \frac{\partial \boldsymbol{f}_{h2}}{\partial \boldsymbol{T}^{i,s}} & \mathbf{0} & \frac{\partial \boldsymbol{f}_{h2}}{\partial \boldsymbol{T}^{i,r}} & \mathbf{0} & \mathbf{0} \\ \mathbf{0} & \mathbf{0} & \frac{\partial \boldsymbol{f}_{h3}}{\partial \boldsymbol{T}^{i,s}} & \frac{\partial \boldsymbol{f}_{h3}}{\partial \boldsymbol{T}^{o,s}} & \frac{\partial \boldsymbol{f}_{h3}}{\partial \boldsymbol{T}^{i,r}} & \frac{\partial \boldsymbol{f}_{h3}}{\partial \boldsymbol{T}^{o,r}} & \mathbf{0} \\ \frac{\partial \boldsymbol{f}_{h4}}{\partial \boldsymbol{T}^s_{nd}} & \frac{\partial \boldsymbol{f}_{h4}}{\partial \boldsymbol{T}^r_{nd}} & \mathbf{0} & \mathbf{0} & \mathbf{0} & \mathbf{0} & \frac{\partial \boldsymbol{f}_{h4}}{\partial \boldsymbol{\phi}} \\ \frac{\partial \boldsymbol{f}_{h5}}{\partial \boldsymbol{T}^s_{nd}} & \mathbf{0} & \mathbf{0} & \mathbf{0} & \mathbf{0} & \mathbf{0} & \frac{\partial \boldsymbol{f}_{h5}}{\partial \boldsymbol{\phi}} \end{bmatrix} \tag{48}$$

where $\boldsymbol{J}_h$ is the Jacobian matrix in the HS.

The decoupling method in the HS analysis involves the following detailed steps, as summarised in Figure 3a.

1. Initialise the supply temperatures of Type II nodes as $T^{s,init}_{nd}$.
2. Solve the equations in the supply network and obtain all the node supply temperatures.
3. Solve the return temperature of the load nodes and then obtain all the node return temperatures.
4. With the return temperature in Step (3), obtain the calculated supply temperature of the Type II node as $\boldsymbol{T}^{s,calc}_{nd}$.
5. If $\boldsymbol{T}^{s,init}_{nd}$ and $\boldsymbol{T}^{s,calc}_{nd}$ satisfy (49), the procedure ends; else turn to Step (6).

$$\max \left| \boldsymbol{T}^{s,init}_{nd,j} - \boldsymbol{T}^{s,calc}_{nd,j} \right| \le \varepsilon \quad j \in \Theta^{sr}_h, j \notin \Theta^{sl}_h \tag{49}$$

where Θ^{sr}_h is the set of the source nodes in the HS.

6. Set $\boldsymbol{T}^{s,calc}_{nd}$ as the initialised supply temperatures of Type II nodes. Return to Step (2).

4.3.2 | Quantity regulation

Under quantity regulation, the HS model is nonlinear and (39) is used. In this mode, the nodes are classified into four types, as shown in Table 4. Types I and II correspond to the source nodes for power and temperature regulation, respectively. Types III and IV correspond to the intermediate and load nodes, respectively.

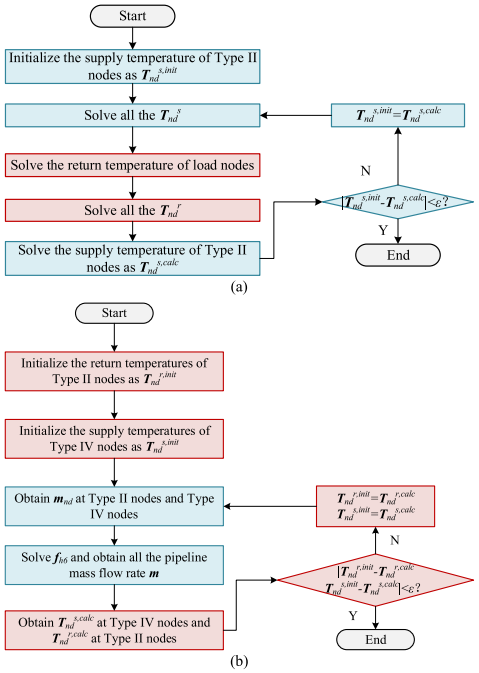

FIGURE 3 Static energy flow analysis in the HS using decoupling method. (a) Energy flow analysis in the quality-regulated HS; (b) energy flow analysis in the quantity-regulated HS. HS, heating system.

TABLE 4 Node variable distribution in quantity-regulated heating system.

Node type	Known variables	Unknown variables
Type I	T^s_{nd}	T^r_{nd}, ϕ
Type II	ϕ, T^s_{nd}	m_{nd}, T^r_{nd}
Type II	ϕ, m_{nd}	T^s_{nd}, T^r_{nd}
Type IV	ϕ, T^r_{nd}	m_{nd}, T^s_{nd}

Despite $3N_h + 4N_{b2}$ variables mentioned in Section 4.3.1, extra $N_h + N_{b2}$ variables are added in the quantity-regulated HS, including N_h node mass flow rate and N_{b2} pipeline mass flow rate. Besides $\boldsymbol{f}_{h1} - \boldsymbol{f}_{h4}$, N_h sets of (18) can be built for mass conservation and N_l sets of (19) can be built for pressure balance (defined as $\boldsymbol{f}_{h6}$). Since $N_{b2} = N_h - 1 + N_l$ according to graph theory, $2N_h - 1$ sets of boundary conditions are additionally needed. Therefore, the boundary condition $\boldsymbol{f}_{h5}$ in quantity-regulated HS is modified as:

$$\begin{cases} T^s_{nd,i} - \varphi_{hT,i} = 0 & i \in \Theta^{sr}_h \\ \phi_{nd,j} - \varphi_{h\phi,j} = 0 & j \in \Theta_h, j \notin \Theta^{sl}_h \\ m_{nd,k} = 0 & i \in \Theta^{int}_h \\ T^r_{nd,b} - \varphi_{hT,b} = 0 & b \in \Theta^{ld}_h \end{cases} \tag{50}$$

where Θ^{int}_h and Θ^{ld}_h are the sets of the intermediate and load nodes in the HS, respectively.

Accordingly, the united method for quantity-regulated HSs differs from for quality-regulated HSs in two aspects. First, $\boldsymbol{m}$

and $\boldsymbol{m}_{nd}$ will be added into $\boldsymbol{u}_h$. Second, $\boldsymbol{f}_{h5}$ in reference (50) and $\boldsymbol{f}_{h6}$ will be used to modify $\boldsymbol{J}_h$. Therefore, the decoupling method for quantity-regulated HSs are modified below, as summarised in Figure 3b.

1. Initialise the return temperatures of Type II nodes as $\boldsymbol{T}_{nd}^{r,init}$ and the supply temperatures of Type IV nodes as $\boldsymbol{T}_{nd}^{s,init}$.
2. Obtain $\boldsymbol{m}_{nd}$ at Type II nodes and Type IV nodes using (24).
3. Solve $\boldsymbol{f}_{h6}$ and obtain all the pipeline mass flow rate $\boldsymbol{m}$.
4. Solve the equations in the supply network and obtain $\boldsymbol{T}_{nd}^{s,calc}$ at Type IV nodes. Solve the equations in the return network and obtain $\boldsymbol{T}_{nd}^{r,calc}$ at Type II nodes.
5. If $\boldsymbol{T}_{nd}^{r,init}$, $\boldsymbol{T}_{nd}^{s,init}$, $\boldsymbol{T}_{nd}^{r,calc}$ and $\boldsymbol{T}_{nd}^{s,calc}$ satisfy (51), the procedure ends; else turn to Step (6).

$$\max \left| \begin{array}{ll} T_{nd,i}^{s,calc} - T_{nd,i}^{s,init} & i \in \Theta_h^{ld} \\ T_{nd,j}^{r,calc} - T_{nd,j}^{r,init} & j \in \Theta_h^{sr}, j \notin \Theta_h^{sl} \end{array} \right| \leq \varepsilon \tag{51}$$

6. Set $\boldsymbol{T}_{nd}^{r,calc}$ as the initialised return temperatures of Type II nodes and $\boldsymbol{T}_{nd}^{s,calc}$ as the initialised supply temperatures of Type IV nodes. Return to Step (2).

4.4 | Analysis in IES

In an IES, the boundary conditions within a subsystem are influenced by other subsystems to some extent. In such cases, a combined analysis is necessary. The framework for IES analysis can be categorised into two types: independent and combined frameworks.

4.4.1 | Independent framework

In this paper, the independent framework refers to an approach wherein subsystems exchange information only once, without iteration or modification. Each subsystem is solved separately, avoiding the need to solve the high-dimensional IES model. This framework is primarily suitable for unidirectionally coupled IES or bidirectional weakly coupled IES, where the coupling units do not participate in power regulation. This configuration is depicted in Figure 4a,b.

4.4.2 | Combined framework

The combined framework in this paper refers to an approach where subsystems share partial or complete information and an iterative and modification process takes place between them. This framework is primarily suitable for bidirectional intensively coupled IES, where the coupling unit functions as a slack node to participate in power regulation. This configuration is depicted in Figure 4c.

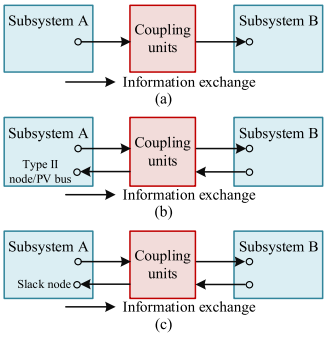

FIGURE 4 Typical structure of IES. (a) Unidirectionally coupled IES; (b) bidirectional weakly coupled IES; (c) bidirectional intensively coupled IES. IES, integrated energy system.

The combined framework with partial information sharing is known as the decoupling method. It solves individual models of each subsystem and the solutions are iteratively adjusted at the coupling units to achieve global convergence. The decoupling method has the following characteristics:

1. It avoids solving the high-dimensional IES model by solving subsystem models separately.
2. Information exchange occurs only at the coupling units, ensuring privacy protection.
3. Developing a universal iteration strategy can be challenging due to different coupling relationships.
4. Iterations between subsystems require significant computational burden and may lead to divergence.

The combined framework with complete information sharing is known as the united method. It combines all the equations and formulates a high-dimensional Jacobian matrix for problem solving, as shown below.

$$\boldsymbol{J}_{cp} = \begin{bmatrix} \boldsymbol{J}_e & \boldsymbol{0} & \boldsymbol{0} & \partial \boldsymbol{f}_e / \partial \boldsymbol{u}_c \\ \boldsymbol{0} & \boldsymbol{J}_g & \boldsymbol{0} & \partial \boldsymbol{f}_g / \partial \boldsymbol{u}_c \\ \boldsymbol{0} & \boldsymbol{0} & \boldsymbol{J}_h & \partial \boldsymbol{f}_h / \partial \boldsymbol{u}_c \\ \partial \boldsymbol{f}_c / \partial \boldsymbol{u}_e & \partial \boldsymbol{f}_c / \partial \boldsymbol{u}_g & \partial \boldsymbol{f}_c / \partial \boldsymbol{u}_h & \partial \boldsymbol{f}_c / \partial \boldsymbol{u}_c \end{bmatrix} \tag{52}$$

where $\boldsymbol{f}_c$ is the vector of equations at coupling units, $\boldsymbol{J}_{cp}$ is the united Jacobian matrix in static analysis.

The typical framework of the united method is shown in Figure 3b. It has the following characteristics:

1. It solves a high-dimensional equation set and requires significant computational cost and storage capacity.
2. It can effectively mitigate the issue of alternating errors.
3. It requires complete information sharing and is not conducive to privacy protection among multiple entities.

5 | METHOD IMPLEMENTATION IN DYNAMIC ANALYSIS

In this section, dynamic GS and HS models from Table 1 are utilised for analysis, introducing two differences compared to static analysis. Firstly, the states at different time steps are interrelated, requiring a sequential analysis. Secondly, the algebraic pipeline models in the GS and HS are replaced with PDEs, which may introduce discrete pipeline variables into the analysis.

5.1 | Analysis in GS

According to Table 1, the mainstream dynamic GS models are described by PDAEs. Thus, the methods described in Section 3.1 are initially required to discretise the pipeline equations, introducing $2(N_x+1)$ variables for each pipeline. In this condition, the variables in the GS include N_g node pressures, N_g node mass flow rates, $\sum(N_x+1)$ pipeline mass flow rates and $\sum(N_x+1)$ pipeline pressures.

Correspondingly, $2N_g+2\sum(N_x+1)$ equations can be built to ensure the closure. Besides $\boldsymbol{f}_{g1}$ and $\boldsymbol{f}_{g3}$, $2N_g$ pressure continuity equations in (10) can be formulated to relate pipeline and node pressures (defined as $\boldsymbol{f}_{g4}$), $\sum N_x$ algebraic continuity equations (defined as $\boldsymbol{f}_{g21}$) and $\sum N_x$ algebraic momentum equations (defined as $\boldsymbol{f}_{g22}$) can be formulated to discretise pipeline equations. Taking *GS-Model2* as an example, $\boldsymbol{f}_{g21}$ and $\boldsymbol{f}_{g22}$ formulated by M1–M3 are given as follows.

M1: FDM with Euler implicit scheme

$$\begin{cases} \dfrac{p_{i+1}^{j+1}-p_{i+1}^{j}}{\Delta t}+\dfrac{c^2}{S}\dfrac{q_{i+1}^{j+1}-q_{i}^{j+1}}{\Delta x}=0 \\ \dfrac{p_{i+1}^{j+1}-p_{i}^{j+1}}{\Delta x}+\dfrac{q_{i+1}^{j+1}-q_{i+1}^{j}}{S\Delta t}+\dfrac{\lambda_g c^2\left(q_{i+1}^{j+1}\right)^2}{2DS^2p_{i+1}^{j+1}}=0 \\ 0\le i\le N_x-1\ ,\quad 0\le j\le N_t-1 \end{cases} \tag{53}$$

M2: FDM with central implicit scheme

$$\begin{cases} \dfrac{p_i^{j+1}+p_{i+1}^{j+1}-p_{i+1}^{j}-p_i^{j}}{\Delta t}+\dfrac{c^2}{S}\dfrac{q_{i+1}^{j}+q_{i+1}^{j+1}-q_i^{j}-q_i^{j+1}}{\Delta x}=0 \\ \dfrac{p_{i+1}^{j}+p_{i+1}^{j+1}-p_i^{j}-p_i^{j+1}}{\Delta x}+\dfrac{q_i^{j+1}+q_{i+1}^{j+1}-q_{i+1}^{j}-q_i^{j}}{S\Delta t} \\ +\dfrac{\lambda c^2}{4DS^2}\left(\dfrac{\left(q_i^{j+1}\right)^2}{p_i^{j+1}}+\dfrac{\left(q_{i+1}^{j+1}\right)^2}{p_{i+1}^{j+1}}+\dfrac{\left(q_i^{j}\right)^2}{p_i^{j}}+\dfrac{\left(q_{i+1}^{j}\right)^2}{p_{i+1}^{j}}\right)=0 \\ 0\le i\le N_x-1\ ,\quad 0\le j\le N_t-1 \end{cases} \tag{54}$$

M3: MOC

$$p_i^{j+1}-p_{i-1}^{j}+\frac{c}{S}\left(q_i^{j+1}-q_{i-1}^{j}\right)+\frac{\lambda_g c^2\Delta x}{4DS^2}\frac{\left(q_i^{j+1}+q_{i-1}^{j}\right)^2}{p_i^{j+1}+p_{i-1}^{j}}=0$$

$$1\le i\le N_x, 0\le j\le N_t-1 \tag{55}$$

$$p_{i+1}^{j}-p_i^{j+1}+\frac{c}{S}\left(q_i^{j+1}-q_{i+1}^{j}\right)+\frac{\lambda_g c^2\Delta x}{4DS^2}\frac{\left(q_i^{j+1}+q_{i+1}^{j}\right)^2}{p_i^{j+1}+p_{i+1}^{j}}=0$$

$$0\le i\le N_x-1, 0\le j\le N_t-1 \tag{56}$$

With the above equations, dynamic energy flow analysis in the GS can be performed. For linear scenarios with *GS-Model4* or *GS-Model5*, Equation (40) is employed. The corresponding vectors and matrixes are as given in Equations (57) and (58). It should be noted that the expressions of $\partial\boldsymbol{f}_{g21}/\partial\boldsymbol{p}$, $\partial\boldsymbol{f}_{g21}/\partial\boldsymbol{q}$, $\partial\boldsymbol{f}_{g22}/\partial\boldsymbol{p}$, $\partial\boldsymbol{f}_{g22}/\partial\boldsymbol{q}$ are determined by the PDE solver and not listed in this paper.

$$\begin{cases} \boldsymbol{u}_g=\begin{bmatrix}\boldsymbol{p}_{nd} & \boldsymbol{q}_{nd} & \boldsymbol{p} & \boldsymbol{q}\end{bmatrix}^{\mathrm{T}} \\ \boldsymbol{f}_g=\begin{bmatrix}\boldsymbol{f}_{g1} & \boldsymbol{f}_{g21} & \boldsymbol{f}_{g22} & \boldsymbol{f}_{g3} & \boldsymbol{f}_{g4}\end{bmatrix}^{\mathrm{T}} \end{cases} \tag{57}$$

$$\boldsymbol{J}_g=\begin{bmatrix} \boldsymbol{0} & \partial\boldsymbol{f}_{g1}/\partial\boldsymbol{q} & \boldsymbol{0} & -\boldsymbol{1} \\ \partial\boldsymbol{f}_{g21}/\partial\boldsymbol{p} & \partial\boldsymbol{f}_{g21}/\partial\boldsymbol{q} & \boldsymbol{0} & \boldsymbol{0} \\ \partial\boldsymbol{f}_{g22}/\partial\boldsymbol{p} & \partial\boldsymbol{f}_{g22}/\partial\boldsymbol{q} & \boldsymbol{0} & \boldsymbol{0} \\ \boldsymbol{0} & \boldsymbol{0} & \partial\boldsymbol{f}_{g3}/\partial\boldsymbol{p}_{nd} & \partial\boldsymbol{f}_{g3}/\partial\boldsymbol{q}_{nd} \\ \partial\boldsymbol{f}_{g4}/\partial\boldsymbol{p} & \boldsymbol{0} & \partial\boldsymbol{f}_{g4}/\partial\boldsymbol{p}_{nd} & \boldsymbol{0} \end{bmatrix} \tag{58}$$

For nonlinear scenarios with *GS-Model1*, *GS-Model2* and *GS-Model3*, Equation (39) is employed for analysis. Meanwhile, $\boldsymbol{u}_g$, $\boldsymbol{f}_g$, $\boldsymbol{J}_g$ in Equations (57) and (58) remain unchanged.

5.2 | Analysis in HS

5.2.1 | Quality regulation

Among various dynamic HS models, *HS-Model1* is described by PDAEs, whereas *HS-Model3* and *HS-Model4* are described by AEs. When utilising *HS-Model3* or *HS-Model4*, the distribution of variables and equations remains the same as that in static analysis and the methods in static analysis in Section 3.3.1 are also suitable for dynamic analysis. The only difference is replacing (25) with (26) or (27) to formulate $\boldsymbol{f}_{h3}$.

As for utilising *HS-Model1*, the methods in Section 3.3.1 are still effective. The only difference is caused by the

discretisation of pipeline equations in PDE form, thereby affecting the distribution of variables and equations. In such cases, (25) is replaced with (59) or (60) or (61) to formulate $\boldsymbol{f}_{h3}$, as shown below.

M1: FDM with Euler implicit scheme

$$\begin{cases} T_{i+1}^{j+1} = \mu_1 T_i^{j+1} + \mu_2 T_{i+1}^{j} & r = C_w m \lambda_h \\ \mu_1 = \dfrac{rv\Delta t}{r\Delta x + rv\Delta t + v\Delta t\Delta x} & 0 \le i \le N_x - 1 \\ & 0 \le j \le N_t - 1 \\ \mu_2 = \dfrac{r\Delta x}{r\Delta x + rv\Delta t + v\Delta t\Delta x} \end{cases} \tag{59}$$

M2: FDM with central implicit scheme

$$\begin{cases} T_{i+1}^{j+1} = \mu_1 T_i^{j} + \mu_2 T_i^{j+1} + \mu_3 T_{i+1}^{j} \\ \mu_1 = \dfrac{2r\Delta x + 2rv\Delta t - v\Delta t\Delta x}{2r\Delta x + 2rv\Delta t + v\Delta t\Delta x} & 0 \le i \le N_x - 1 \\ \mu_2 = \dfrac{-2r\Delta x + 2rv\Delta t - v\Delta t\Delta x}{2r\Delta x + 2rv\Delta t + v\Delta t\Delta x} & 0 \le j \le N_t - 1 \\ \mu_3 = \dfrac{2r\Delta x - 2rv\Delta t - v\Delta t\Delta x}{2r\Delta x + 2rv\Delta t + v\Delta t\Delta x} \end{cases} \tag{60}$$

M3: MOC

$$T_{i+1}^{j+1} = \frac{2r - \Delta x}{2r + \Delta x} T_i^{j} \quad \begin{matrix} 0 \le i \le N_x - 1 \\ 0 \le j \le N_t - 1 \end{matrix} \tag{61}$$

Accordingly, (47) and (48) are modified as:

$$\begin{cases} \boldsymbol{u}_h = \left[\boldsymbol{T}_{nd}^{s} \quad \boldsymbol{T}_{nd}^{r} \quad \boldsymbol{T}^{s} \quad \boldsymbol{T}^{r} \quad \boldsymbol{T}_{nd}^{r} \right]^{\mathrm{T}} \\ \boldsymbol{f}_h = \left[\boldsymbol{f}_{h1} \quad \boldsymbol{f}_{h2} \quad \boldsymbol{f}_{h3} \quad \boldsymbol{f}_{h4} \quad \boldsymbol{f}_{h5} \right]^{\mathrm{T}} \end{cases} \tag{62}$$

$$\boldsymbol{J}_h = \begin{bmatrix} \partial \boldsymbol{f}_{h1}/\partial \boldsymbol{T}_{nd}^{s} & \partial \boldsymbol{f}_{h1}/\partial \boldsymbol{T}_{nd}^{s} & \partial \boldsymbol{f}_{h1}/\partial \boldsymbol{T}^{s} & \partial \boldsymbol{f}_{h1}/\partial \boldsymbol{T}^{r} & \boldsymbol{0} \\ \partial \boldsymbol{f}_{h2}/\partial \boldsymbol{T}_{nd}^{s} & \partial \boldsymbol{f}_{h2}/\partial \boldsymbol{T}_{nd}^{r} & \partial \boldsymbol{f}_{h2}/\partial \boldsymbol{T}^{s} & \partial \boldsymbol{f}_{h2}/\partial \boldsymbol{T}^{r} & \boldsymbol{0} \\ \boldsymbol{0} & \boldsymbol{0} & \partial \boldsymbol{f}_{h3}/\partial \boldsymbol{T}^{s} & \partial \boldsymbol{f}_{h3}/\partial \boldsymbol{T}^{r} & \boldsymbol{0} \\ \partial \boldsymbol{f}_{h4}/\partial \boldsymbol{T}_{nd}^{s} & \partial \boldsymbol{f}_{h4}/\partial \boldsymbol{T}_{nd}^{r} & \boldsymbol{0} & \boldsymbol{0} & \partial \boldsymbol{f}_{h4}/\partial \boldsymbol{\phi} \\ \partial \boldsymbol{f}_{h5}/\partial \boldsymbol{T}_{nd}^{s} & \boldsymbol{0} & \boldsymbol{0} & \boldsymbol{0} & \partial \boldsymbol{f}_{h5}/\partial \boldsymbol{\phi} \end{bmatrix} \tag{63}$$

Also, the decoupling method for dynamic energy flow analysis in quality-regulated HSs is accordingly modified, as shown in Figure 5a.

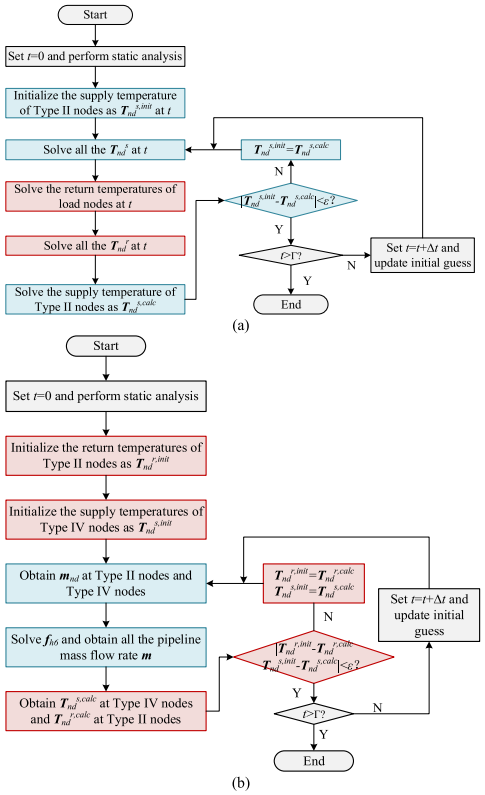

FIGURE 5 Dynamic energy flow analysis in the HS using decoupling method. (a) Energy flow analysis in the quality-regulated HS; (b) energy flow analysis in the quantity-regulated HS. HS, heating system.

5.2.2 | Quantity regulation

In the context of quantity-regulated HS, the methods for static analysis are similar to dynamic analysis with a few differences. These differences can be summarised as follows.

1. *Pipeline equations.* The static pipeline equation in *HS-Model2* is replaced with those in the dynamic models. Correspondingly, $\boldsymbol{u}_h$, $\boldsymbol{f}_{h3}$ and $\boldsymbol{J}_h$ are modified according to the used model.
2. *Updating the initial guess at each time step.* In dynamic analysis, the initial guess for the nonlinear problem needs to be updated at each time step. There are two common methods to determine the initial guess for dynamic analysis. The first method involves performing a static analysis at each time step and the obtained results are used as the initial guess for the dynamic analysis. The second method uses the results of the static analysis as the initial guess for the dynamic analysis at $t = 0$ and then the results of the dynamic analysis at time t are used as the initial guess at $t = t + 1$.

With these differences, the decoupling method and united method can be adjusted accordingly. Regarding the decoupling method, the detailed steps are modified as follows and the procedure is summarised in Figure 5b.

1. Set $t = 0$ and perform the static analysis.

2. The results in Step (1) are used as initial guesses for dynamic analysis at $t = 0$.
3. Obtain $\boldsymbol{m}_{nd}$ of Type II nodes and Type IV nodes at t.
4. Solve $\boldsymbol{f}_{h6}$ and obtain all the pipeline mass flow rate $\boldsymbol{m}$ at t.
5. Solve the equations in the supply network and obtain $\boldsymbol{T}_{nd}^{s,calc}$ at Type IV nodes at t. Solve the equations in the return network and obtain $\boldsymbol{T}_{nd}^{r,calc}$ at Type II nodes at t.
6. If $\boldsymbol{T}_{nd}^{r,init}$, $\boldsymbol{T}_{nd}^{s,init}$, $\boldsymbol{T}_{nd}^{r,calc}$ and $\boldsymbol{T}_{nd}^{s,calc}$ satisfy (51), turn to Step (7); else turn to Step (6).
7. Set $\boldsymbol{T}_{nd}^{r,calc}$ as the initialised return temperatures of Type II nodes and $\boldsymbol{T}_{nd}^{s,calc}$ as the initialised supply temperatures of Type IV nodes. Return to Step (3).
8. If $t > \Gamma$, the procedure ends. Else, set $t = t + \Delta t$ and the results of Step (4) as the initial guess at t, return to Step (3).

5.2.3 | Analysis in IES

Likewise, the frameworks in Section 4.4 also apply to dynamic energy flow analysis. The differences lie that the static models of HS and GS should be replaced with the dynamic models in the framework, along with the corresponding solutions. The comparisons between the static and dynamic analysis in IESs are illustrated in Figure 6.

6 | CASE STUDY-MODEL ILLUSTRATIONS AND METHOD IMPLEMENTATIONS

This section presents a comprehensive comparison between various IES models. As the PS model is relatively mature in IES, the comparison mainly focuses on the GS and HS models. Overall, six widely-used cases are investigated in different scenarios, including 3 HSs and 3 GSs. All the case data (system topology, simulation settings, initial guesses, detailed results, etc.) are open-source for reproducing and further utilisation.

6.1 | Comparisons of GS models

In this section, three cases are presented, including a 11-node GS, a 27-node GS and a 133-node GS, as shown in Figure 7. Case 1 and Case 3 are collected from GasLib.[28] Case 2 is modified from reference 10. The data of three cases are summarised in reference 29. We would like to emphasise that each model has its corresponding applicable scenarios. This case study aims to showcase the simulation results of different methods and guide their implementation for scholars, rather than highlighting the comparison between different models. To illustrate the comparisons more convincingly, M2 is firstly used to solve dynamic GS models considering its applicability. Specifically, w in *GS-Model4* and *GS-Model5* is calculated according to the methods in reference 3. *GS-Model6* is solved with NR method in Equation (39). The three GSs operate with constant pressure boundaries. The number of time steps is 720. The simulation step sizes are shown in Table 4. ε is 10^{-3} in both static and dynamic analysis.

6.1.1 | Case 1: 11-node GS

The more detailed simulation settings and results are open-source in reference 30. The results are summarised in the *Case1-Result* file *M2-GS* document, including node variables and pipeline variables at each time step. The initial guesses at

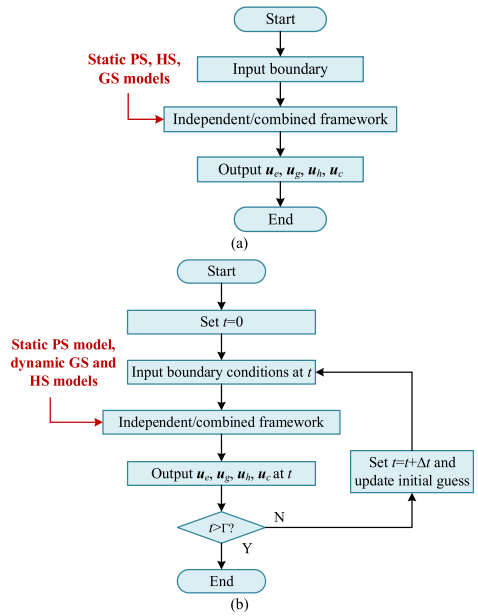

FIGURE 6 Energy flow analysis in IESs. (a) Static energy flow analysis in IESs; (b) dynamic energy flow analysis in IESs. IESs, integrated energy systems.

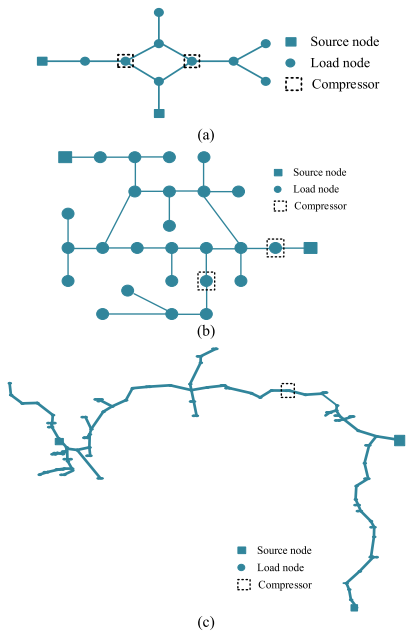

FIGURE 7 Test cases of gas systems. (a) GS-Case 1; (b) GS-Case 2; (c) GS-Case 3. GS, gas system.

each time step are provided in the *Case1-Settings* file. Some of the Jacobian matrixes $\boldsymbol{J}_g$ during the iterative process are provided in the *Case1-Matrix* file for references. Specifically, $\boldsymbol{J}_g$ in *GS-Model4* and *GS-Model5* is constant, while that in the other models vary at each time step.

Figure 8a–d depicts some of the simulation results. Based on the simulations, it can be observed that neglecting the convection and acceleration terms has a negligible impact on the simulation results in the given scenario. However, neglecting the nonlinearity and dynamics of gas flow leads to significant differences. In static models, the simulation results are independent of Δt and are solely determined by the boundary conditions. In this case, the results of static models reflect the stable states of the variations and keep the same stepped trajectory as boundary conditions. Nevertheless, these simplifications contribute to improving efficiency, as they reduce the dimension of $\boldsymbol{J}_g$ in *GS-Model6* and eliminate the need for matrix inversion in *GS-Model4* and *GS-Model5*.

6.1.2 | Case 2: 27-node GS

The detailed results and settings in Case 2 are summarised in the same manner and provided in the Case2-related files in reference 30. The performance comparisons in Case 2 are similar to those in Case 1. The difference is that the dimension of pipeline variables in Case 2 is much larger than that in Case 1, making the complexity comparison between dynamic and static models more distinct. Some of the simulation results are presented in Figure 9.

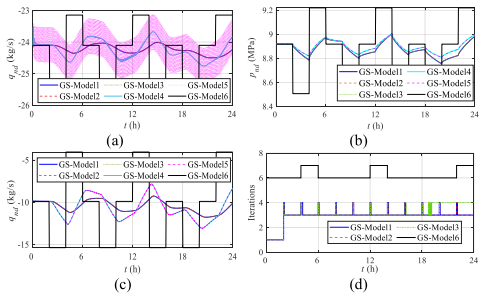

FIGURE 8 Results in GS-Case 1. (a) $q_{nd,1}$; (b) $p_{nd,11}$; (c) $q_{nd,2}$; (d) number of iterations. GS, gas system.

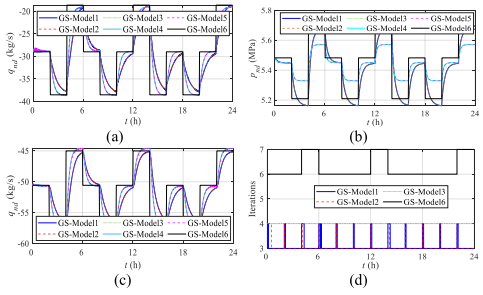

FIGURE 9 Results in GS-Case 2. (a) $q_{nd,1}$; (b) $p_{nd,27}$; (c) $q_{nd,20}$; (d) number of iterations. GS, gas system.

6.1.3 | Case 3: 133-node GS

Similarly, the results and settings in Case 3 are open-source in reference 30. According to Figure 10c, the mass flow rate at sources becomes positive during several periods in the static model and is impractical, while those in dynamic models remain negative. This emphasises the significance of modelling gas flow dynamics in the GS. Moreover, the complexity caused by pipeline discretisation is more significant than the former two cases, resulting in a considerable computation burden in dynamic energy flow analysis.

6.2 | Solution comparisons in GS

With the three GSs, M1 and M3 are also implemented in energy flow analysis for references. The simulation settings in this part are almost the same as Section 4.1. The difference is that the Courant-Friedrichs-Lewy (CFL) condition[15] restricts the selection of Δx and Δt in M3. Thus, M3 is unsuitable for Case 2 and Case 3 and is only implemented in Case 1, as summarised in Table 5. The results and settings of M1 and M3 are provided in the *M1-GS* and *M3-GS* documents in reference 30. It should be noted that M1 diverges in Case 3, hence, the corresponding results are not provided.

6.3 | Comparisons of HS models

Three cases in this section include a 35-node HS, a 51-node HS and a 225-node HS, as shown in Figure 11. Three cases are obtained from,[4,8,9] respectively. The data of three cases are provided in reference 29. The HSs are assumed to operate under quality regulation mode because four HS models mainly differ in thermal part. The decoupling method is used to solve the HS models. The temperature distribution in *HS-Model3* and *HS-Model4* when $t - \xi < 0$ is set as the initial condition. The simulation period is 24 h and Δt is 120 s. The analytical method in reference 31 is used to solve *HS-Model1*, which can avoid the potential numerical fluctuations caused by FDM. ε is 10^{-3}°C in both static and dynamic analysis.

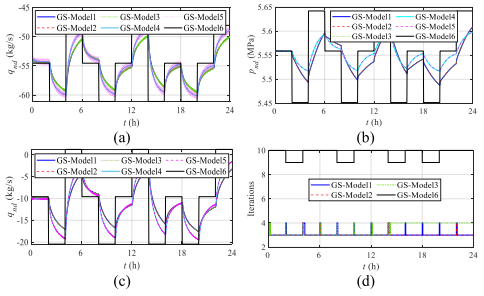

FIGURE 10 Results in GS-Case 3. (a) $q_{nd,20}$; (b) $p_{nd,133}$; (c) $q_{nd,79}$; (d) number of iterations. GS, gas system.

TABLE 5 Simulation steps of three methods in the gas systems.

Case	M1	M2	M3
1	$\Delta x = 2500$ m, $\Delta t = 120$ s	$\Delta x = 2500$ m, $\Delta t = 120$ s	$\Delta x = 11{,}000$ m, $\Delta t = 30$ s
2	$\Delta x = 1000$ m, $\Delta t = 120$ s	$\Delta x = 500$ m, $\Delta t = 120$ s	Unsuitable for GS with short pipelines
3	$\Delta x = 500$ m, $\Delta t = 120$ s	—	

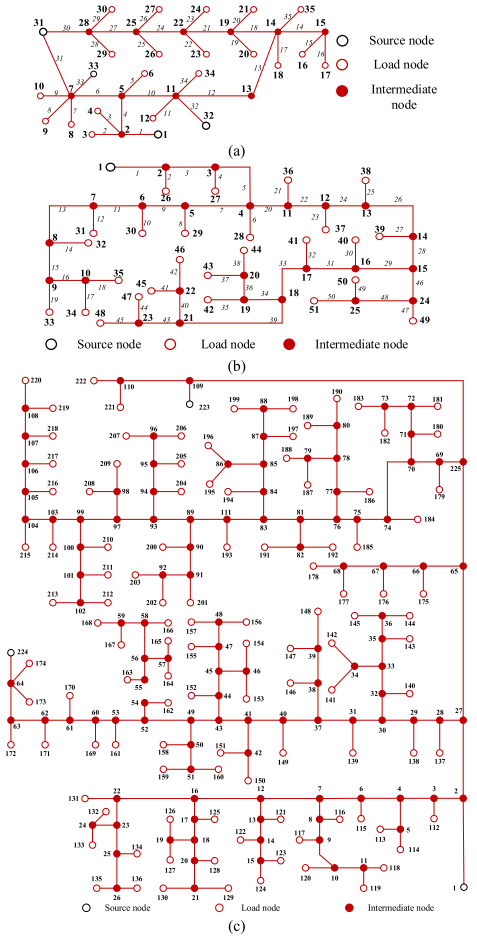

FIGURE 11 Test cases of heating systems. (a) HS-Case 1; (b) HS-Case 2; (c) HS-Case 3. HS, heating system.

6.3.1 | Case 1: 35-node HS

In this case, node 31 is the Type I node for power regulation, while nodes 1 and 32 are the Type II nodes for temperature regulation. The detailed simulation settings and results are open-source in reference 32 and summarised in the *Case1-Result* file in the *HS-Model* document, including node supply and return temperatures at each time step. The initial guesses at each time step are provided in the *Case1-Settings* file. Figure 11a–c depicts some of the simulation results. According to the simulations, we can find that the results of *HS-Model1*, *HS-Model3* and *HS-Model4* are almost the same. The differences between the three dynamic models mainly

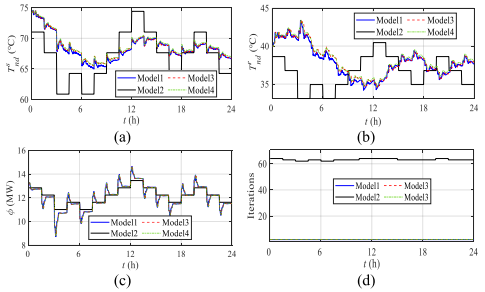

FIGURE 12 Results in HS-Case 1. (a) $T^{s}_{nd,1}$; (b) $T^{r}_{nd,32}$; (c) ϕ_{31}; (d) number of iterations. HS, heating system.

exist in the early stage. This is because the temperature distribution when $t - \xi < 0$ is set as the initial condition in *HS-Model3* and *HS-Model4*, while that in *HS-Model1* is determined by both initial condition and the corresponding transfer loss.

In contrast, the simulated temperatures of *HS-Model2* exhibit noticeable disparities compared to the dynamic models. Despite the simplification of the $\partial T/\partial t$ term causing a delay in temperature variations in the dynamic models, the simulated thermal power remains nearly identical, particularly when the temperature variation stabilises, as depicted in Figure 12c. This can be attributed to the fact that the representation of temperature loss in static models is not simplified and closely resembles that of dynamic models. This characteristic renders static models suitable for relatively coarse analyses that prioritise computational efficiency, such as scenario reduction in planning problems.

6.3.2 | Case 2: 51-node HS

In this case, node 1 is the Type I node for power regulation. The results and settings are summarised in the *Case2-Result* file of the *HS-Model* document.[32] Some of the results are shown in Figure 13. According to Figure 13a,d, the results of the *HS-Model2* distinctly lag behind those of *HS-Model1*, *HS-Model3* and *HS-Model4*. The time delay varies between different nodes. For instance, the distance between nodes 1 and 26 is longer than that between nodes 1 and 51, causing the time delay in Figure 13a larger than that in Figure 13d.

6.3.3 | Case 3: 225-node HS

In this case, node 223 is the Type I node for power regulation, while nodes 1 and 224 are the Type II nodes for temperature regulation. The results are summarised in the *Case3-Result* file of the *HS-Model* document,[32] part of which is shown in Figure 14. The comparisons between four models are similar to those in Cases 2 and 3. However, the decoupling method converges much slowly in *HS-Model2*. In such cases, the united method may be a better solution.

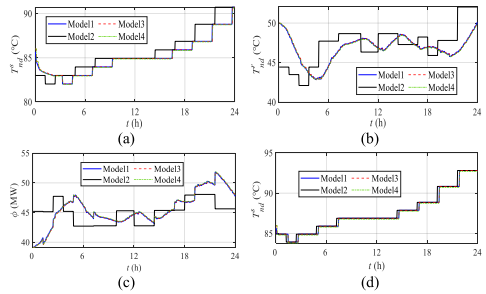

FIGURE 13 Results in HS-Case 2. (a) $T^{s}_{nd,51}$; (b) $T^{r}_{nd,1}$; (c) ϕ_1; (d) $T^{s}_{nd,26}$. HS, heating system.

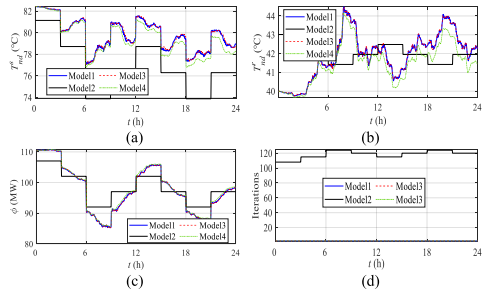

FIGURE 14 Results in HS-Case 3. (a) $T^{s}_{nd,225}$; (b) $T^{r}_{nd,1}$; (c) ϕ_{223}; (d) number of iterations. HS, heating system.

TABLE 6 Simulation steps of three methods in the heating systems.

Case	1	2	3
Δx	50 m	50 m	200 m
Δt	120 s	120 s	120 s

6.4 | Solution comparisons in HS

With the three HSs, M1, M2 and M3 are also adopted to solve the PDEs in *HS-Model1* for illustration. The simulation steps are shown in Table 6. The detailed results are open-source in the *M1-Result*, *M2-Result* and *M3-Result* files in the *HS-Methods* documents for reference 32.

7 | CASE STUDY-ANALYSIS OF IES

This section focuses on the method implementations in the IES for benchmarking. The analysis is performed in a large-scale IES composed of a 118-bus PS, a 225-node HS and a 133-node GS. The 118-bus PS is modified from the IEEE 118-bus test system. The 225-node HS and 133-node GS are from Section 4. Three systems are coupled with one back-pressure CHP unit, two EBs, five GTs and one P2G. The parameters and structure of the two cases are given in reference 29 and Figure 15, respectively. To balance the modelling accuracy and complexity, *GS-Model2* and *HS-Model1* are adopted to model the GS and HS, respectively. M2 and analytical methods in reference 31 are used to solve GS and HS models. The simulation period is 24 h and Δt is 120 s.

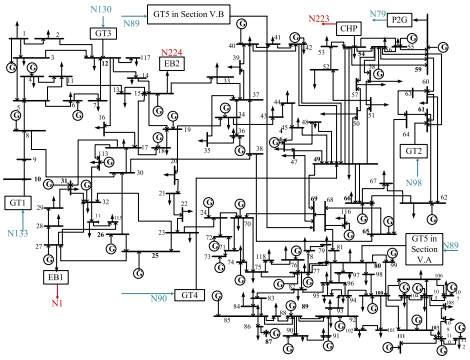

FIGURE 15 Structure of the integrated energy system.

Since our target is to illustrate the differences between the independent and combined frameworks in IES analysis, the coupling relationships between the subsystems are different in the following two sections. To be specific, nodes 1, 223 and 224 in the HS are connected to buses 27, 54 and 15 in the PS, wherein buses 27 and 224 are PQ buses and bus 54 is PV bus. Nodes 79, 90, 98, 130 and 133 in the GS are connected to buses 59, 49, 61, 12 and 10 in the PS, wherein buses 49, 61, 12 and 10 are PV buses and bus 59 is PQ bus. In Section 6.1, node 89 in the GS is connected to bus 80 in the PS, wherein bus 80 is the PV bus. In Section 6.2, node 89 in the GS is connected to bus 69 in the PS, wherein bus 69 is the slack bus.

7.1 | Independent framework

In this section, GT5 is connected to bus 80 in the PS and works as the PV bus. The system in Figure 14 is a bidirectional weakly coupled IES, wherein no iterations or modifications exist between the subsystems. The scholars can first solve the GS and HS models to obtain the operational boundaries and then solve the PS model. The detailed results and settings are summarised in the *IES1-Results* and *IES1-Settings* file for reference 33. Some of the results are depicted in Figure 16.

7.2 | Combined framework

In this section, GT5 is connected to bus 69 in the PS and works as the slack bus. The system in Figure 15 is a bidirectional intensively coupled IES, wherein the results in the GS and PS need to iterate until converge. The scholars can perform the energy flow analysis using the decoupling method, which involves the following steps.

1. Solve the HS models to obtain the active power generation at bus 64 and active power load at buses 27 and 15.
2. Initialise the mass flow rate of node 89.
3. Perform the dynamic energy flow analysis in the GS.

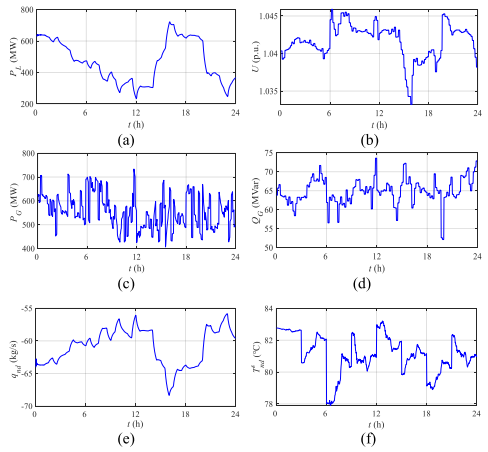

FIGURE 16 Results in bidirectional weakly coupled integrated energy system. (a) $P_{L,59}$; (b) U_9; (c) $P_{G,69}$; (d) $Q_{G,12}$; (e) $q_{nd,1}$; (f) $T^s_{nd,1}$.

4. According to the mass flow rate in Step (2), determine the active power generation of the slack bus as $P^{init}_{G,69}$.
5. Obtain the active power load at bus 58 and active power generations at buses 49, 61, 12 and 10.
6. Perform power flow analysis and obtain the calculated active power generation of the slack bus as $P^{calc}_{G,69}$.
7. Determine whether $\left|P^{init}_{G,69} - P^{calc}_{G,69}\right| \leq \varepsilon$ holds. If so, the calculations at this time step ends. Else, turn to Step (8).
8. Re-initialise the mass flow rate of node 89 using $P^{calc}_{G,69}$ and return to Step (3).

The detailed results and settings are summarised in the *IES2-Results* and *IES21-Settings* file in reference 32 for reference. Some of the results are depicted in Figure 17. Specifically, Figure 17g refers to the iterations between Step (2) and Step (8) at each time step. Figure 17h refers to the iterations inside Step (2) at each time step.

8 | CONCLUSIONS

This paper offers a comprehensive analysis of IES from both modelling and solution perspectives. A detailed overview of mainstream IES models and their interrelationships are presented, including six GS models and four HS models. Additionally, several widely used solvers for PDEs and AEs are introduced, along with their applications in different subsystems of IES. Specifically, their applications in the GSs and HSs are further categorised according to the nonlinear and dynamic features. These models and methods are also implemented in different test systems for illustration. The system data, simulation settings, computational processes and detailed results are shared as open-source, allowing scholars to easily design and validate their own specific IES analyses. Moreover, scholars have the flexibility to choose appropriate models for specific scenarios, considering factors such as computational time, numerical performance and solvability requirements. In this context, the results and solution process presented in this paper can serve as valuable references by adjusting the simulation settings.

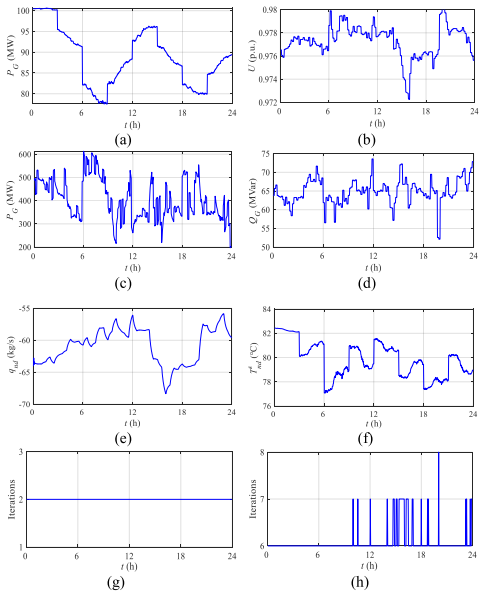

FIGURE 17 Results in bidirectional intensively coupled IES. (a) $P_{G,54}$; (b) U_{43}; (c) $P_{G,69}$; (d) $Q_{G,40}$; (e) $q_{nd,20}$; (f) $T^s_{nd,224}$; (g) iterations in IES; (h) iterations in GS. GS, gas system; IES, integrated energy system.

Overall, this paper serves as a valuable resource for scholars seeking a comprehensive understanding of existing methods for IES analysis and can facilitate customised investigations and reproducibility in future research.

AUTHOR CONTRIBUTIONS

Suhan Zhang: Writing – original draft. **Wei Gu:** Supervision. **X.-P. Zhang:** Conceptualization. **C. Y. Chung:** Writing – review & editing. **Ruizhi Yu:** Validation. **Shuai Lu:** Writing – review & editing. **Rodrigo Palma-Behnke:** Investigation.

ACKNOWLEDGEMENTS

This work was supported by The National Science Fund for Distinguished Young Scholars (52325703) and also by the IEEE Power and Energy Society Working Group on Test Systems for Economic Analysis.

CONFLICT OF INTEREST STATEMENT

The authors declare that they have no known competing financial interests or personal relationships that could have appeared to influence the work reported in this paper.

DATA AVAILABILITY STATEMENT

The data that support the findings of this study are openly available in the manuscript.

REFERENCES

1. Ramsebner, J., R. Haas, H. Auer, A. Ajanovic, W. Gawlik, C. Maier, S. Nemec-Begluk, T. Nacht, and M. Puchegger. 2021. "From Single to Multi-Energy and Hybrid Grids: Historic Growth and Future Vision." *Renewable and Sustainable Energy Reviews* 151: 111520. https://doi.org/10.1016/j.rser.2021.111520.

2. Wu, J., J. Yan, H. Jia, N. Hatziargyriou, N. Djilali, and H. Sun. 2016. "Integrated Energy Systems." *Applied Energy* 167: 155–7. https://doi.org/10.1016/j.apenergy.2016.02.075.
3. Zhang, S., W. Gu, X. Zhang, H. Lu, R. Yu, H. Qiu, and S. Lu. 2022. "Dynamic Modeling and Simulation of Integrated Electricity and Gas Systems." *IEEE Transactions on Smart Grid* 14(2): 1011–26. https://doi.org/10.1109/tsg.2022.3203485.
4. Liu, X., J. Wu, N. Jenkins, and A. Bagdanavicius. 2016. "Combined Analysis of Electricity and Heat Networks." *Applied Energy* 162: 1238–50. https://doi.org/10.1016/j.apenergy.2015.01.102.
5. Shabanpour, A., and A. R. Seifi. 2016. "An Integrated Steady-State Operation Assessment of Electrical, Natural Gas and District Heating Networks." *IEEE Transactions on Power Systems* 31(5): 3636–47. https://doi.org/10.1109/tpwrs.2015.2486819.
6. Zhang, G., F. Zhang, K. Me, X. Zhang, and Z. Y. Dong. 2020. "A Fixed-point Based Distributed Method for Energy Flow Calculation in Multi-Energy Systems." *IEEE Transactions on Sustainable Energy* 11(4): 2567–80. https://doi.org/10.1109/tste.2020.2966737.
7. Massrur, H., T. Niknam, J. Aghae, M. Shafie-Khah, and J. P. S. Catalao. 2018. "Fast Decomposed Energy Flow in Large-Scale Integrated Electricity-Gas-Heat Energy Systems." *IEEE Transactions on Sustainable Energy* 9(4): 1565–77. https://doi.org/10.1109/tste.2018.2795755.
8. Zhang, S., W. Gu, S. Yao, S. Lu, S. Zhou, and Z. Wu. 2021. "Partitional Decoupling Method for Fast Calculation of Energy Flow in a Large-Scale Heat and Electricity Integrated Energy System." *IEEE Transactions on Sustainable Energy* 12(1): 501–13. https://doi.org/10.1109/tste.2020.3008189.
9. Zhang, S., W. Gu, S. Lu, H. Qiu, S. Lu, D. Wang, J. Liang, and W. Li. 2021. "Superposition-Principle Based Decoupling Method for Energy Flow Calculation in District Heating Networks." *Applied Energy* 295: 117032. https://doi.org/10.1016/j.apenergy.2021.117032.
10. Fang, J., Q. Zeng, X. Ai, Z. Chen, and J. Wen. 2018. "Dynamic Optimal Energy Flow in the Integrated Natural Gas and Electrical Power Systems." *IEEE Transactions on Sustainable Energy* 9(1): 188–98. https://doi.org/10.1109/tste.2017.2717600.
11. Yao, S., W. Gu, S. Lu, S. Zhou, Z. Wu, G. Pan, and D. He. 2021. "Dynamic Optimal Energy Flow in the Heat and Electricity Integrated Energy System." *IEEE Transactions on Sustainable Energy* 12(1): 179–90. https://doi.org/10.1109/tste.2020.2988682.
12. Yang, J., N. Zhang, C. Kang, and Q. Xia. 2018. "Effect of Natural Gas Flow Dynamics in Robust Generation Scheduling under Wind Uncertainty." *IEEE Transactions on Power Systems* 33(3): 2087–97. https://doi.org/10.1109/tpwrs.2017.2733222.
13. Qin, X., H. Sun, X. Shen, Ye Guo, Q. Guo, and T. Xia. 2019. "A Generalized Quasi-Dynamic Model for Electric-Heat Coupling Integrated Energy System with Distributed Energy Resources." *Applied Energy* 251: 113270. https://doi.org/10.1016/j.apenergy.2019.05.073.
14. Zhang, S., W. Gu, S. Yao, Z. Wu, and S. Zhou. 2021. "Unified Modeling of Integrated Energy Networks in Time Domain and its Applications (I): Two-Port Models in Time Domain." *Proceedings of the CSEE* 41(19): 6509–20.
15. Zhang, S., W. Gu, X. Zhang, S. Lu, R. Yu, H. Lu, S. Zhao, and J. Wang. 2023. "Towards Fast and Robust Simulation in Integrated Electricity and Gas System: A Sequential United Method." *IEEE Transactions on Power Systems* 39(1): 1822–36. https://doi.org/10.1109/TPWRS.2023.3240394.
16. Chen, Y., Q. Guo, H. Sun, Z. Pan, and B. Chen. 2021. "Generalized Phasor Modeling of Dynamic Gas Flow for Integrated Electricity-Gas Dispatch." *Applied Energy* 283: 116153. https://doi.org/10.1016/j.apenergy.2020.116153.
17. Chen, Y., Q. Guo, H. Sun, and Z. Pan. 2021. "Integrated Heat and Electricity Dispatch for District Heating Networks with Constant Mass Flow: A Generalized Phasor Method." *IEEE Transactions on Power Systems* 36(1): 426–37. https://doi.org/10.1109/tpwrs.2020.3008345.
18. Chen, B., Q. Guo, G. Yin, B. Wang, Z. Pan, Y. Chen, W. Wu, and H. Sun. 2022. "Energy-Circuit-Based Integrated Energy Management System: Theory, Implementation and Application." *Proceedings of the IEEE* 110(12): 1897–926. https://doi.org/10.1109/jproc.2022.3216567.
19. Yang, J., N. Zhang, A. Botterud, and C. Kang. 2020. "Situation Awareness of Electricity-Gas Coupled Systems with a Multi-Port Equivalent Gas Network Model." *Applied Energy* 258: 114029. https://doi.org/10.1016/j.apenergy.2019.114029.
20. Yang, J., N. Zhang, A. Botterud, and C. Kang. 2020. "On an Equivalent Representation of the Dynamics in District Heating Networks for Combined Electricity-Heat Operation." *IEEE Transactions on Power Systems* 35(1): 560–70. https://doi.org/10.1109/tpwrs.2019.2935748.
21. Huang, W., N. Zhang, Y. Cheng, J. Yang, Yi Wang, and C. Kang. 2020. "Multienergy Networks Analytics: Standardized Modeling, Optimization and Low Carbon Analysis." *Proceedings of the IEEE* 108(9): 1411–36. https://doi.org/10.1109/jproc.2020.2993787.
22. Liu, Y., and K. Sun. 2020. "Solving Power System Differential Algebraic Equations Using Differential Transformation." *IEEE Transactions on Power Systems* 35(3): 2289–99. https://doi.org/10.1109/tpwrs.2019.2945512.
23. Yu, R., W. Gu, H. Lu, S. Yao, S. Zhang, S. Lu, S. Ding, and E. Luo. 2023. "Non-iterative Calculation of Quasi-Dynamic Energy Flow in the Heat and Electricity Integrated Energy Systems." *IEEE Transactions on Power Systems* 38(5): 4148–64. https://doi.org/10.1109/tpwrs.2022.3210167.
24. Li, J., D. Wang, H. Jia, Y. Lei, T. Zhou, and Y. Guo. 2022. "Mechanism Analysis and Unified Calculation Model of Exergy Flow Distribution in Regional Integrated Energy System." *Applied Energy* 324: 119725. https://doi.org/10.1016/j.apenergy.2022.119725.
25. Qin, X., X. Shen, Y. Guo, Z. Pan, Q. Guo, and H. Sun. 2021. "Combined Electric and Heat System Testbeds for Power Flow Analysis and Economic Dispatch." *CSEE JPES* 7(1): 34–44.
26. Vladimir, D., Z. Branislav, P. Sanja, B. Maslovaric, V. Karamarkovic, and V. Trkulja. 2009. "Prediction of Thermal Transients in District Heating Systems." *Energy Conversion and Management* 50(9): 2167–73. https://doi.org/10.1016/j.enconman.2009.04.034.
27. Courant, R., and K. Friedrichs. 1956. *Supersonic Flow and Waves*. London: Interscience Publishers.
28. Schmidt, M., D. Aßmann, R. Burlacu, J. Humpola, I. Joormann, N. Kaneakis, T. Koch, et al. 2017. "GasLib A Library of Gas Network Instances." [Online]. http://gaslib.zib.de/.
29. Zhang, S., and R. Yu. 2024. "System Data." [Online]. https://github.com/wgu-101/IES-benchmark-cases/tree/main/System%20data.
30. Zhang, S., and R. Yu. 2024. "Data of GS Data of GS in Section V.A&B." [Online]. https://github.com/wgu-101/IES-benchmark-cases/tree/main/Data%20of%20GS%20in%20Section%20V.A%26B.
31. Zhang, S., W. Gu, X. Zhang, H. Lu, S. Lu, R. Yu, and H. Qiu. 2022. "Fully Analytical Model of Heating Networks for Integrated Energy Systems." *Applied Energy* 327: 120081. https://doi.org/10.1016/j.apenergy.2022.120081.
32. Zhang, S., and R. Yu. 2024. "Data of GS Data of HS in Section V.C&D." [Online]. https://github.com/wgu-101/IES-benchmark-cases/tree/main/Data%20of%20HS%20in%20Section%20V.C%26D.
33. Zhang, S., and R. Yu. 2024. "Data in Section VI." [Online]. https://github.com/wgu-101/IES-benchmark-cases/tree/main/Data%20in%20Section%20VI.